Dentate network activity is necessary for spatial working memory by supporting CA3 sharp-wave ripple generation and prospective firing of CA3 neurons

Takuya Sasaki[1,2,3], Verónica C. Piatti[1], Ernie Hwaun[1], Siavash Ahmadi[1], John E. Lisman[4], Stefan Leutgeb [1,5] and Jill K. Leutgeb [1*]

Complex spatial working memory tasks have been shown to require both hippocampal sharp-wave ripple (SWR) activity and dentate gyrus (DG) neuronal activity. We therefore asked whether DG inputs to CA3 contribute to spatial working memory by promoting SWR generation. Recordings from DG and CA3 while rats performed a dentate-dependent working memory task on an eight-arm radial maze revealed that the activity of dentate neurons and the incidence rate of SWRs both increased during reward consumption. We then found reduced reward-related CA3 SWR generation without direct input from dentate granule neurons. Furthermore, CA3 cells with place fields in not-yet-visited arms preferentially fired during SWRs at reward locations, and these prospective CA3 firing patterns were more pronounced for correct trials and were dentate-dependent. These results indicate that coordination of CA3 neuronal activity patterns by DG is necessary for the generation of neuronal firing patterns that support goal-directed behavior and memory.

Working memory (WM) is the ability to temporarily store and process information that is relevant for completing goal-directed actions. Based on the profound behavioral performance deficits in complex spatial WM tasks after DG lesions, the projections of DG granule cells to CA3 through the mossy fiber (MF) pathway have been considered to be critical for WM tasks with delays of tens of seconds to hours[1]. The finding that spatial firing patterns of dentate cells show pattern separation[2,3] has led to the suggestion that DG projections to CA3 support memory by promoting the generation of distinct hippocampal firing patterns. However, the DG–CA3 network is also characterized by recurrent connections, both directly between CA3 cells and more indirectly between dentate granule cells, hilar mossy cells and CA3 cells[4,5]. These dense direct and indirect recurrent pathways in the DG–CA3 network form associative circuits that have been suggested to be critical for retaining complex spatial WM[6,7].

Furthermore, the CA3 region, whether independently[8,9] or by modulation from the CA2 region[10], is thought to initiate SWRs, which then propagate from CA3 to CA1. SWRs are prominent hippocampal network oscillations (150–250 Hz) that are observed during sleep as well as during periods of immobility in awake behavior[11]. SWRs are characterized by short bouts of increased neuronal activity during which time-compressed sequences are replayed, which correspond to sequential activity patterns that are observed on a longer time scale in behavior[12–16]. The reactivation of sequential activity patterns during SWRs is thought to underlie processes important for memory such as consolidation and retrieval[17–19]. In particular, it has been shown that selective elimination of awake SWRs in

hippocampus impairs future route planning[20] and behavioral performance in a spatial WM task[21]. This suggests that SWR-associated reactivation of hippocampal cell ensembles during ongoing behavior is a potential mechanism for maintaining representations of stored items for use in planning future choices in WM.

There is evidence that SWRs do not occur during periods of low DG granule cell activity[22] and, conversely, that CA3 and hilar neuronal activity is increased in parallel during SWRs[8–10,23,24]. These correlations, together with the findings that SWRs and dentate inputs to CA3 are both critical for spatial WM, led us to investigate whether DG inputs to CA3 may contribute to spatial WM by effects on SWR generation and on ripple-related neuronal firing patterns. Therefore, in a task in which DG is necessary for WM performance, we recorded neuronal firing patterns in DG and CA3 and examined to what extent CA3 network activity patterns and ripple-associated firing patterns of individual CA3 cells were dependent on DG inputs.

Results

Dentate granule neurons were necessary for spatial WM in the eight-arm radial maze. We first confirmed that our version of the spatial WM task was dependent on the DG. Rats ($n = 16$) were trained to perform an eight-arm radial maze task in which reward was available at the end of each of the arms (Fig. 1a). In the first phase of each trial, four arms were sequentially presented in a pseudorandom order (forced phase). In the second phase, all arms were made accessible, such that the animal had to remember and choose the arms where reward was still available (choice phase). The optimal strategy is to visit each arm only once per trial. A trial with at

[1]Neurobiology Section and Center for Neural Circuits and Behavior, Division of Biological Sciences, University of California, San Diego, La Jolla, CA, USA. [2]Laboratory of Chemical Pharmacology, Graduate School of Pharmaceutical Sciences, The University of Tokyo, Tokyo, Japan. [3]Precursory Research for Embryonic Science and Technology, Japan Science and Technology Agency, Kawaguchi, Japan. [4]Department of Biology, Brandeis University, Waltham, MA, USA. [5]Kavli Institute for Brain and Mind, University of California, San Diego, La Jolla, CA, USA. Takuya Sasaki and Verónica C. Piatti contributed equally to this work. Deceased: John E. Lisman. *e-mail: jleutgeb@ucsd.edu
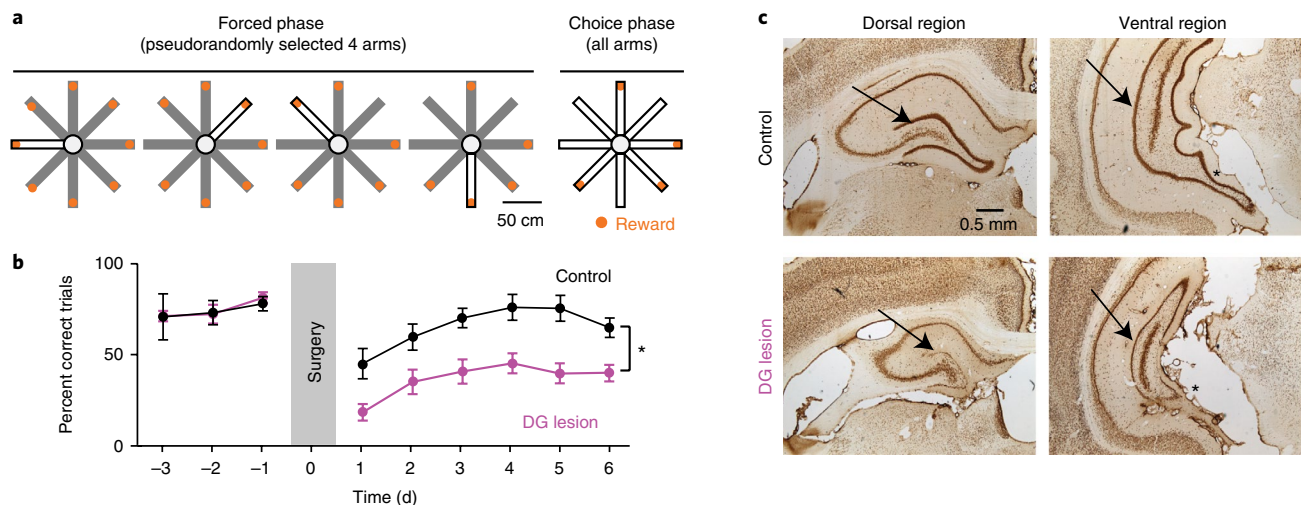
Fig. 1 | Selective dentate granule cell lesions impaired spatial working memory. a, A spatial WM task was performed on an eight-arm radial maze with reward locations (orange) at the end of each arm. Four arms were individually presented during the forced phase, after which all arms were made available in the choice phase. Open and closed arms in the schematic are shown in white and gray, respectively. **b**, Mean ($\pm$ s.e.m.) percent correct performance in the spatial WM task as a function of testing day. Selective pharmacological lesions of dentate granule neurons with colchicine resulted in significant memory impairment ($n = 5$ control rats, 11 lesioned rats; $F_{1,70} = 16.07$, $P = 0.0013$, repeated-measures ANOVA; *$P < 0.05$, comparison between groups). **c**, Coronal brain sections of the dorsal and ventral hippocampus labeled with NeuN in a control rat (top) and a DG-lesioned rat (bottom). Sections from control and DG-lesioned rats are at the same coordinates from bregma. Arrows point to the dentate granule cell layer. Asterisks highlight the reduction in ventral DG volume in the lesion compared to control rat.

least one reentry into an arm was therefore considered an incorrect trial. Initial training on the task was performed for 30 min (6–10 trials) per day until at least 50% of trials were correct over 5 consecutive days (days to criterion: 15.1 ± 2.4, $n = 16$ animals; Fig. 1b and Supplementary Fig. 1a). After reaching criterion, dentate granule cells were selectively lesioned with bilateral infusions of colchicine (six sites per hemisphere; see Online Methods)[1] throughout the entire septotemporal axis of the hippocampus in 11 of the 16 animals (Fig. 1c). The remaining five animals underwent sham surgery and served as controls. In the lesioned rats ($n = 11$), there was a $73.7 \pm 1.4\%$ (range: 59.0% to 82.4%) reduction of the volume in the DG granule cell layer, as quantified using the Cavalieri method (Supplementary Fig. 1c,d).

During behavioral testing after surgery, control animals performed the majority of all trials without errors. In contrast, all animals with DG lesions showed a striking deficit in their ability to choose correct arms (percent correct trials, range over 6 d: 18.4% to 45.3% in 11 DG-lesioned rats vs. 39.6% to 78.2% in 5 control rats, $F_{1,70} = 16.07$, $P = 1.3 \times 10^{-3}$; Fig. 1b; number of errors, range over 6 d: 2.5–1.0 in 11 DG-lesioned rats vs. 1.5–0.3 in 5 control rats, $F_{1,70} = 6.55$, $P = 0.023$, repeated-measures ANOVA over 6 d after surgery; Supplementary Fig. 1a). Some errors were committed during the first choice after the forced phase (0.03 ± 0.01 errors per choice in control and 0.18 ± 0.04 in DG-lesioned rats), but the likelihood of errors increased for later choices (fourth choice: 0.11 ± 0.02 errors per choice in control and 0.26 ± 0.03 in DG-lesioned rats), when a higher number of previous choices needed to be remembered (Supplementary Fig. 1b). Despite the difference in overall error levels, control and lesioned rats therefore appeared to use a strategy for which the number of past choices increased the likelihood of future errors. Furthermore, we confirmed that damage to the entire CA1 and CA3 was not substantial ($21.3 \pm 2.9\%$ and $12.1 \pm 1.9\%$, respectively) in DG-lesioned rats. While damage to dorsal CA1 and CA3 ($31.9 \pm 3.6\%$ and $19.6 \pm 2.1\%$) was larger compared to ventral damage ($6.4 \pm 5.6\%$ and $8.7 \pm 3.5\%$), neither dorsal nor ventral damage were correlated with spatial memory performance in DG-lesioned rats (Supplementary Fig. 1c).

Dentate cells were selectively active at reward locations. To examine neuronal firing patterns that may contribute to spatial WM performance, we recorded DG cells in 8 rats during the WM task ($n = 71$ cells, including 24 cells from the granule cell layer and 47 from the hilus; Fig. 2a,b and Supplementary Fig. 2). As previously reported, we found that many active dentate cells (>0.01 Hz, $n = 62$ of 71) had spatially selective activity patterns on maze arms or on the center platform (22.6%, 14 of 62 cells). The proportion of spatially selective cells during WM approximately corresponded to the proportion identified during random foraging (RF) on the eight-arm maze (30.6%, 15 of 49 active cells), although field locations did not match between the tasks (Supplementary Fig. 3a). Consistent with recent reports[25–27], place-selectivity was more typical for DG cells recorded from sites in the hilus than for cells in the granule cell layer (Fig. 2c–e). In addition to standard spatial firing on the maze, we also observed in WM that the firing rates of many dentate cells were higher on arm ends than in the inner portion of the maze (> 1.5-fold more active: 37 of 62 cells, 59.7%; median: 6.9-fold; Fig. 2c). Arm-end selectivity could occur either on a limited set of arm ends (spatially selective; 23 of 37 cells; Fig. 2d,e) or without a consistent arm preference (14 of 37 cells). Arm-end selective firing was most typical for recording sites located in the dentate granule cell layer. Therefore, the firing patterns of the majority of active DG cells in WM differed substantially from those of standard place cells.

Because dentate cells recorded in the granule cell layer fired predominantly at the reward locations in the spatial WM task, we examined the precise pattern of dentate spiking in more detail and recorded an additional 16 arm-end selective dentate cells (in two rats) with sensors that signaled precisely when rats were licking the reward (Fig. 2f). For all analysis of reward-related neuronal activity patterns, only the initial visit to each of the eight arms was included; repeat visits were excluded. Dentate cells with firing rates >0.01 Hz (12 of 16 cells, mean rate: 0.022 ± 0.016 Hz) showed activity that was on average 18.4-fold higher after contact compared to before contact with the reward (range: 4.4- to 69.5-fold). Throughout the approximately 3-s period while rats consumed the reward, average dentate firing rates increased gradually (Fig. 2g).
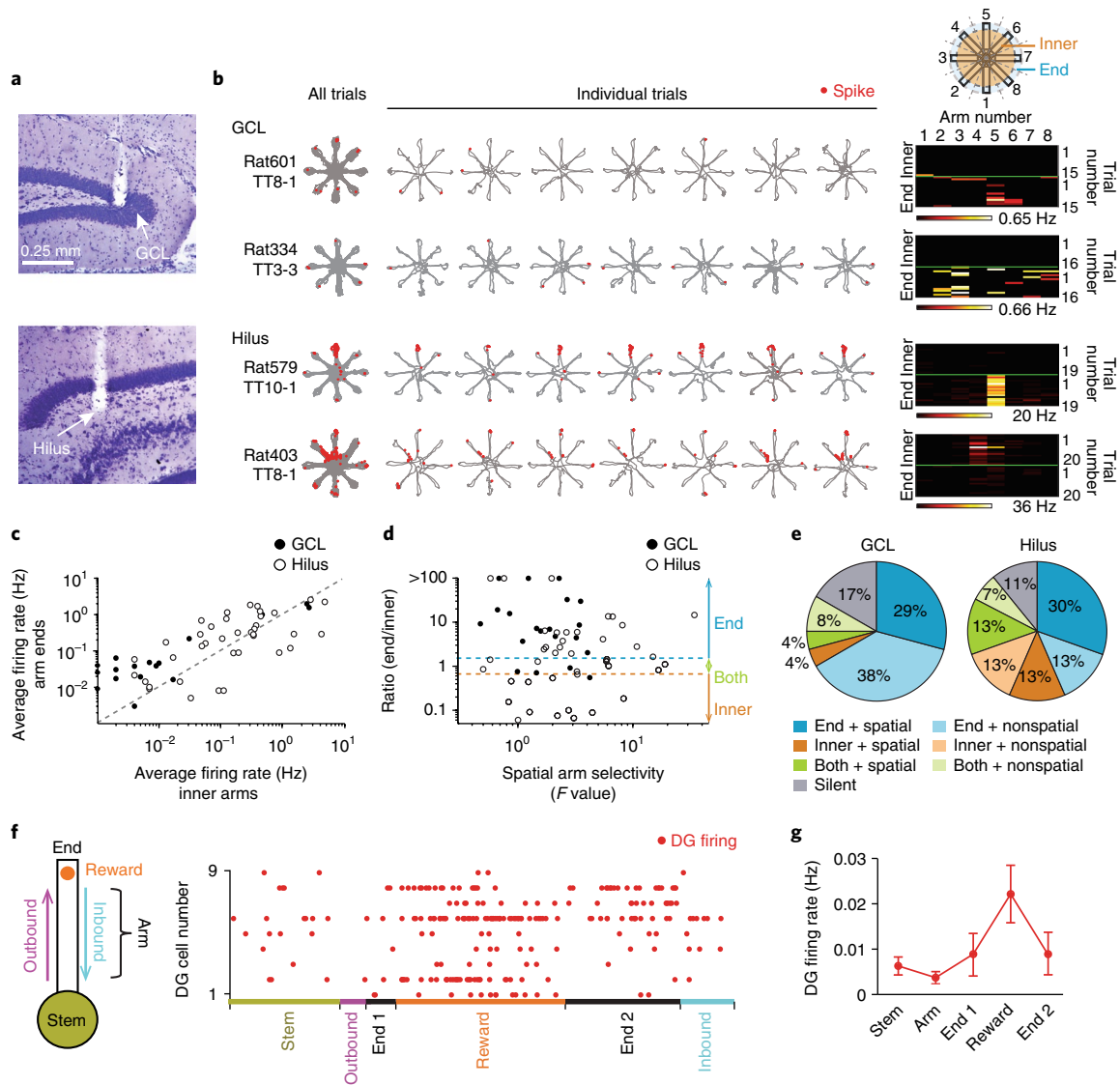
Fig. 2 | Reward-selective firing of dentate cells. a, Histological confirmation of recording sites (white arrows) in the DG granule cell layer (GCL, top) and the hilus (bottom) in a cresyl-stained section. **b**, Representative firing patterns of cells recorded from the GCL and hilus in the spatial WM task. Similar results were obtained in 24 GCL and 47 hilus cells from 8 control rats and are quantified in panels **c**–**e**. Each row is the activity pattern of a single dentate neuron. The trajectories (gray) with spike locations (red dots) are shown superimposed for all trials in a recording session and separately for the first 7 of up to 20 trials (from left to right). Rightmost: color-coded matrices summarizing the firing pattern of the example cells over the entire spatial WM session. Firing rate is represented by a color scale from zero (black) to the highest peak in the session (white, corresponding to the number at the bottom of each matrix). The top half of the matrix corresponds to the firing rates on the arms ('inner') and the bottom half to the firing on the arm ends ('end'). Note that two distinct types of firing patterns are evident in these matrices: either location-selective firing across trials (hilus, Rat 579, TT10-1; hilus, Rat 403, TT8-1) or selective firing at a subset of reward locations (GCL, Rat 601, TT8-1; GCL, Rat 334, TT3-3). **c**, Average firing rates of dentate cells on the maze arms compared to the arm ends ($n = 24$ GCL cells, filled circles; and 47 hilus cells, open circles). Each dot is a single dentate cell. **d**, The ratio of the firing rate at the arm ends to that in the maze arms is plotted against a statistical measure of arm selectivity (F value from ANOVA with rate by arm and trials as factors). Dotted blue and orange lines represent ratios of 3/2 and 2/3, respectively, which correspond to the cutoffs for selectivity to arm ends and inner arms. Cells with ratios between these two values were considered active in both segments. **e**, Proportion of dentate neurons classified based on the plot in **d**. Cells with an average firing rate < 0.01 Hz on the maze were defined as silent cells. Cells with $P < 0.05$ in the ANOVA were defined as spatial cells. **f**, Firing of example dentate cells during distinct periods within each trial. Periods are defined and colored coded as indicated in the schematic on the left, and the arm end was divided into the time before, during and after reward consumption (arm end 1, reward and arm end 2, respectively). The length of each behavioral period in the illustration corresponds to its average duration in a trial. **g**, Average frequency (± s.e.m.) of behavior-related DG cell spikes ($n = 16$ cells). Increased firing occurred during reward consumption.

SWRs in CA3 preferentially occurred at reward locations. We then examined whether the increased DG activity during reward periods in WM was associated with distinct CA3 local field potential (LFP) patterns. We began by evaluating the running speed in different sections of the maze and found that periods of immobility and low running velocities only occurred on the arm ends (Fig. 3a–c). This region of the maze was characterized by SWRs (Fig. 3d–f) that preferentially occurred during the period while rats consumed the reward ($n = 4$ control rats, during reward: 0.151 ± 0.023 Hz; during immobility before and after reward: 0.042 ± 0.012 Hz and
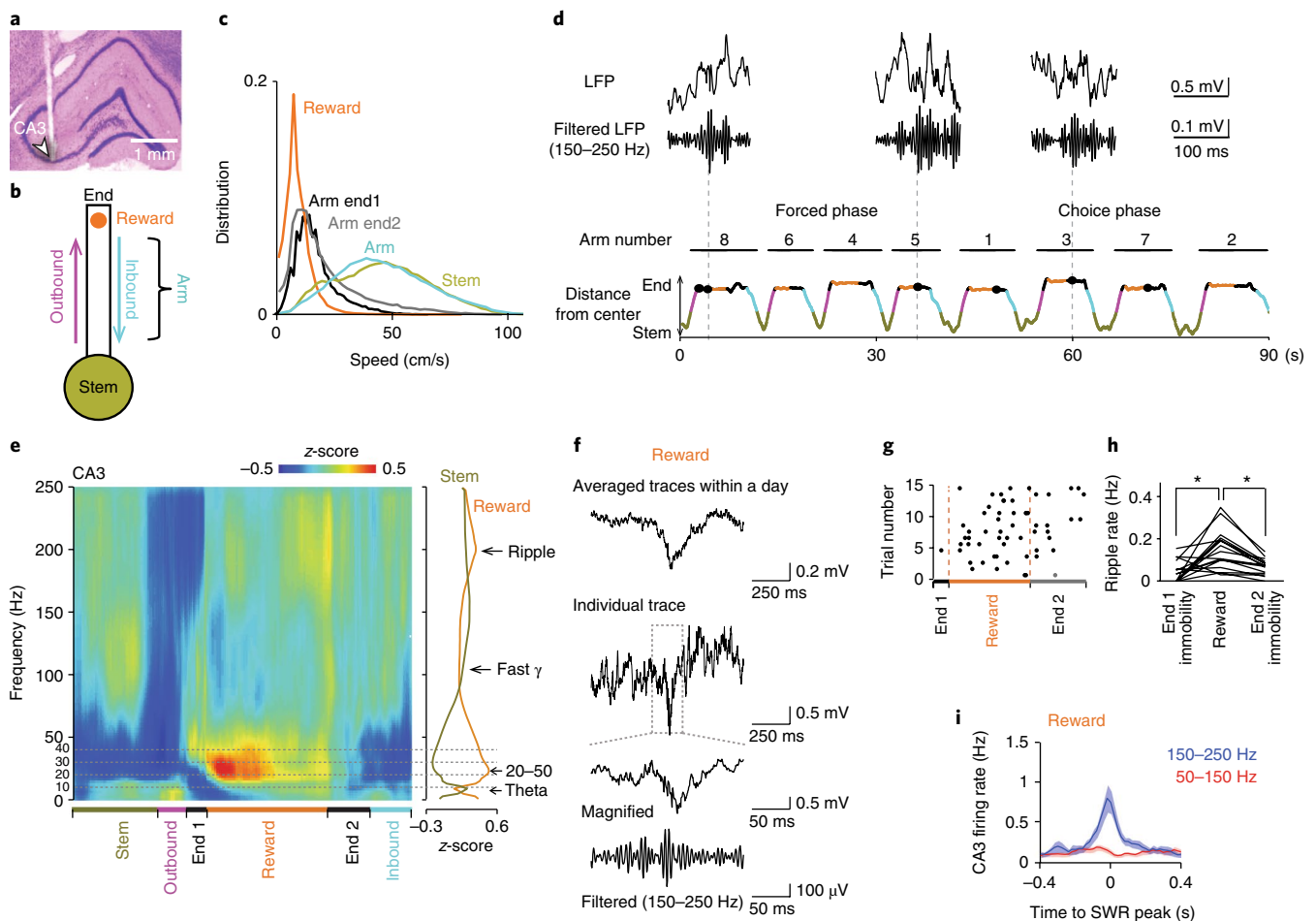
Fig. 3 | CA3 ripple events during the spatial WM task. a, Histological confirmation of a CA3 recording site (indicated by arrow). **b**, Schematic of behavioral periods. **c**, Running speed distribution for the periods defined in **b**. Data from 4 control rats with reward sensors were combined. Immobility and low running speeds were only observed on arm ends (before, during and after reward consumption). **d**, SWR events at arm ends plotted by time within the trial and distance from the center of the maze. Behavioral periods are colored as in **b**. Unfiltered and bandpass-filtered (150–250 Hz) LFP traces of example high-frequency events are shown on top. Vertical stippled lines indicate correspondence to the timeline. **e**, Left: LFP power spectrogram from a CA3 recording site. Trials from one recording day were averaged. Progression through behavioral periods is indicated at the bottom. Right: average LFP power during reward and stem periods as a function of frequency ($n = 18$ trials, 8 reward periods per trial). The peak frequencies were in the 20- to 50-Hz range and in the 150- to 250-Hz range during reward consumption but in the theta range at the stem. See Supplementary Fig. 7a–c for related analyses. **f**, Averages of all SWR events in the session (top; $n = 111$ events) and an individual event (middle; see Supplementary Fig. 8a for additional examples from other animals and the average over all animals). Bottom: expansion of the boxed region in the individual event. **g**, Occurrence of SWRs in all trials of a recording day. For visualization of the distribution over multiple trials, each behavioral period within a trial was normalized to the average length of the corresponding period. CA3 SWRs primarily occurred during reward consumption. **h**, Comparison of SWR rates between periods of reward consumption and immobility at arm ends ($n = 17$ tetrodes from 4 animals, reward vs. periods of end immobility, $F_{2,48} = 13.07$, $P = 2.9 \times 10^{-5}$, ANOVA; $P < 0.01$, Scheffé test). Each line represents a CA3 recording site; *$P < 0.05$. **i**, Event-triggered firing rate (mean ± s.e.m. for each 20-ms bin) for CA3 pyramidal cells ($n = 116$ from 17 tetrodes in 4 animals). LFP signals were bandpass-filtered in two separate frequency bands (50–150 Hz and 150–250 Hz), and events detected when the root-mean-square power of the filtered traces exceeded 3 s.d. above the mean.

0.071 ± 0.009 Hz, respectively; $n = 17$ tetrodes, reward vs. immobility before: $t_{16} = 4.00$, $P = 0.0020$; reward vs. immobility after: $t_{16} = 5.10$, $P = 2.2 \times 10^{-4}$, paired t tests; Fig. 3g,h and Supplementary Figs. 4–8). The reward-related increase in incidence rate was observed irrespective of the amplitude threshold for SWRs (from >3 s.d. to > 5 s.d.; Supplementary Fig. 5). Furthermore, the incidence rate of ripples at reward sites was higher during correct compared to incorrect trials for the choice phase but not the forced phase of the task (choice, correct: 0.16 ± 0.02 Hz; incorrect: 0.12 ± 0.02 Hz, $t_{16} = 2.13$, $P = 0.049$, paired t test; forced, correct: 0.18 ± 0.03 Hz; incorrect: 0.20 ± 0.02 Hz, $t_{16} = 0.92$, $P = 0.37$, paired t test; Supplementary Fig. 9b). More frequent reward-associated CA3 ripples during the choice phase were thus correlated with more accurate WM processing.

To evaluate whether SWRs at reward locations qualitatively corresponded to awake ripples, we confirmed that the firing rates of individual CA3 cells were low before ripple events and increased several-fold during ripple events ($n = 116$ cells, before: 0.13 ± 0.02 Hz; during: 0.73 ± 0.14 Hz; Fig. 3i and Supplementary Fig. 7e). Such transient surges in hippocampal firing rates from a low baseline level correspond to patterns that have previously been reported for SWRs during wakefulness and sleep[9,10,28–30].

Dentate network activity was necessary for reward-associated increases in CA3 SWRs. To more directly investigate whether the reward-related increase in CA3 SWRs and CA3 neuronal activity depended on dentate inputs, we performed dorsal CA3 recordings
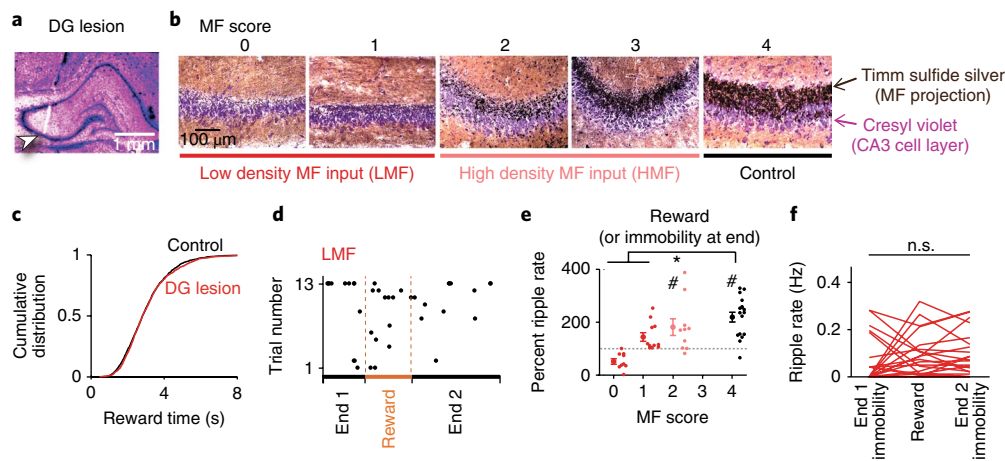
Fig. 4 | Reward-associated CA3 SWR events were dependent on direct MF input from DG. a, Histological confirmation of a CA3 recording site in a DG-lesioned rat (indicated by arrow). **b**, MF density was scored at each recording site in the hippocampal CA3 subregion on a scale from 0 (no MF input) to 4 (control MF input). Scores 0–1 were combined into the LMF group and higher scores comprised the HMF group. Cell bodies are labeled with cresyl violet (purple), and MF of dentate granule cells are labeled with Timm stain (black). **c**, Cumulative distribution of duration of reward intake ($n = 1,521$ and 1,585 reward events in control and lesioned rats, respectively; $D_{max} = 0.032$, $P = 0.42$, Kolmogorov–Smirnov test). **d**, As in Fig. 3g but for an LMF CA3 recording site in a DG-lesioned animal. **e**, Percent ripple event rates during reward compared to periods of immobility on arm ends for each CA3 recording site (dots represent individual CA3 recording sites, grouped by MF score; score 0: $n = 9$ from 6 animals, $t_8 = 0.24$, $P = 0.81$; score 1: $n = 11$ from 6 animals, $t_{10} = 0.72$, $P = 0.49$; score 2: $n = 10$ from 5 animals, $t_9 = 2.71$, $P = 0.024$; score 4: $n = 17$ from 4 animals, $t_{16} = 4.99$, $P = 1.3 \times 10^{-4}$; two-sided paired t test within the group; control vs. LMF, $U = 211$, $Z = 3.71$, $P = 2.0 \times 10^{-4}$; control vs. HMF, $U = 116$, $Z = 1.18$, $P = 0.24$, two-sided Mann–Whitney U test followed by post hoc Bonferroni corrections). The choice and forced phases are combined (see Supplementary Fig. 9 for additional related analyses). *$P < 0.05$, comparison across groups; #$P < 0.05$, reward vs. immobility at end within group. **f**, For the LMF group, ripple rates did not increase during reward compared to other immobile periods at arm ends ($n = 20$ tetrodes from 9 DG-lesioned animals; $F_{2,57} = 0.67$, $P = 0.52$, ANOVA).

in 4 control and 10 DG-lesioned rats (Fig. 4a–f and Supplementary Fig. 10). Even though our DG lesion size was substantial along the entire dorsoventral extent of the DG, we scored the extent of remaining MF innervation at each CA3 recording location based on Timm's sulfide silver-positive signals in the CA3 striatum lucidum (Fig. 4b; scores from 0 to 4: no detectable density, low density, moderate density, near-complete density and control density, respectively; see Online Methods for a detailed description). For analysis of electrophysiological signals, sites with scores of 0–1 were combined into the low-density MF input (LMF) group and sites with scores of 2 or higher comprised the high-density MF input (HMF) group. There were no CA3 recording sites in lesioned rats with a score higher than 2.

We first confirmed that DG lesions did not result in any differences in behavioral patterns in the spatial WM task, including the time spent at the reward location (Fig. 4c and Supplementary Table 1). We next observed that reward-related SWR rates were reduced at many but not all CA3 recording sites (Fig. 4d–f) and therefore tested whether the heterogeneous effects could be explained by the degree of residual MF projections. At LMF sites, SWRs did not show the typical increase in incidence rates during the reward period, while HMF sites showed an increase in SWRs during the reward period comparable to those in control CA3 sites (range for control sites: 63% to 328%, median = 235%; range for LMF sites: 0% to 252%, median = 101%; range for HMF sites: 80% to 388%, median = 169%; control vs. LMF, $U = 453$, $Z = 3.95$, $P = 7.9 \times 10^{-5}$; control vs. HMF, $U = 262$, $Z = 1.18$, $P = 0.24$, Mann–Whitney U test; Fig. 4e and see Supplementary Fig. 9c–e for additional detail). The lack of reward-related increase in SWR rates was also observed for the raw ripple rates at LMF sites ($n = 20$ tetrodes; $F_{2,57} = 0.42$, $P = 0.42$, ANOVA; Fig. 4f). Differences between low- and high-density MF groups were apparent even within a single DG-lesioned animal (Supplementary Fig. 9f), but differences depending on remaining CA1 volume, CA3 volume or recording location within CA3 were not observed (Supplementary Fig. 11). In addition, we

analyzed high-frequency oscillations during rest and found that SWRs were affected to a similar extent as those at reward locations (Supplementary Fig. 12).

Reward-associated 20- to 50-Hz oscillations at CA3 recording sites were DG-dependent. To determine whether reward-related oscillations other than SWRs were affected by DG lesions, CA3 LFP spectrograms were further analyzed. In control recordings, we found that fast gamma (65–140 Hz) power was low at reward sites compared to oscillations in the 20- to 50-Hz band, which sharply increased during reward consumption ($n = 17$ tetrodes; reward vs. all other behavior, $P < 0.01$, Scheffé test; Figs. 3e and 5a,c–e). The power increase in the 20- to 50-Hz band was significantly greater when associated with reward than while the animals simply paused without taking reward (reward: 0.28 ± 0.04; immobility at arm end: 0.06 ± 0.04, control, $t_{16} = 8.91$, $P = 5.8 \times 10^{-8}$, paired t test; Supplementary Fig. 4f) and could thus not be explained by the onset of immobility[31]. In addition, LFP coherence between DG and CA3 selectively increased in the 20- to 50-Hz band during reward consumption ($n = 35$ tetrode pairs, reward vs. all other behavior: $P < 0.01$, Scheffé test; Fig. 5b), consistent with the possibility that these oscillations in CA3 depended on intact dentate granule cells or that the signal was volume-conducted from DG to CA3. We found that the reward-associated increase in 20- to 50-Hz power was significantly lower at LMF recording sites in DG-lesioned animals compared to control animals (control: $n = 17$ tetrodes, range: 0.04 to 1.06, median = 0.48; HMF: $n = 10$ tetrodes, range: −0.10 to 0.66, median = 0.17; LMF: $n = 20$ tetrodes, range: −0.31 to 0.70, median = 0.24; control vs. HMF, $U = 288$, $Z = 2.49$, $P = 0.26$; control vs. LMF, $U = 431$, $Z = 3.28$, $P = 2.0 \times 10^{-4}$, Mann–Whitney U test followed by post hoc Bonferroni corrections; Fig. 5f–i).

The increase in both 20- to 50-Hz power and SWR rates at reward sites in controls, along with the dentate dependence of both types of oscillations, raised the question whether these oscillations were coupled. Contrary to evidence for coupling, we found that
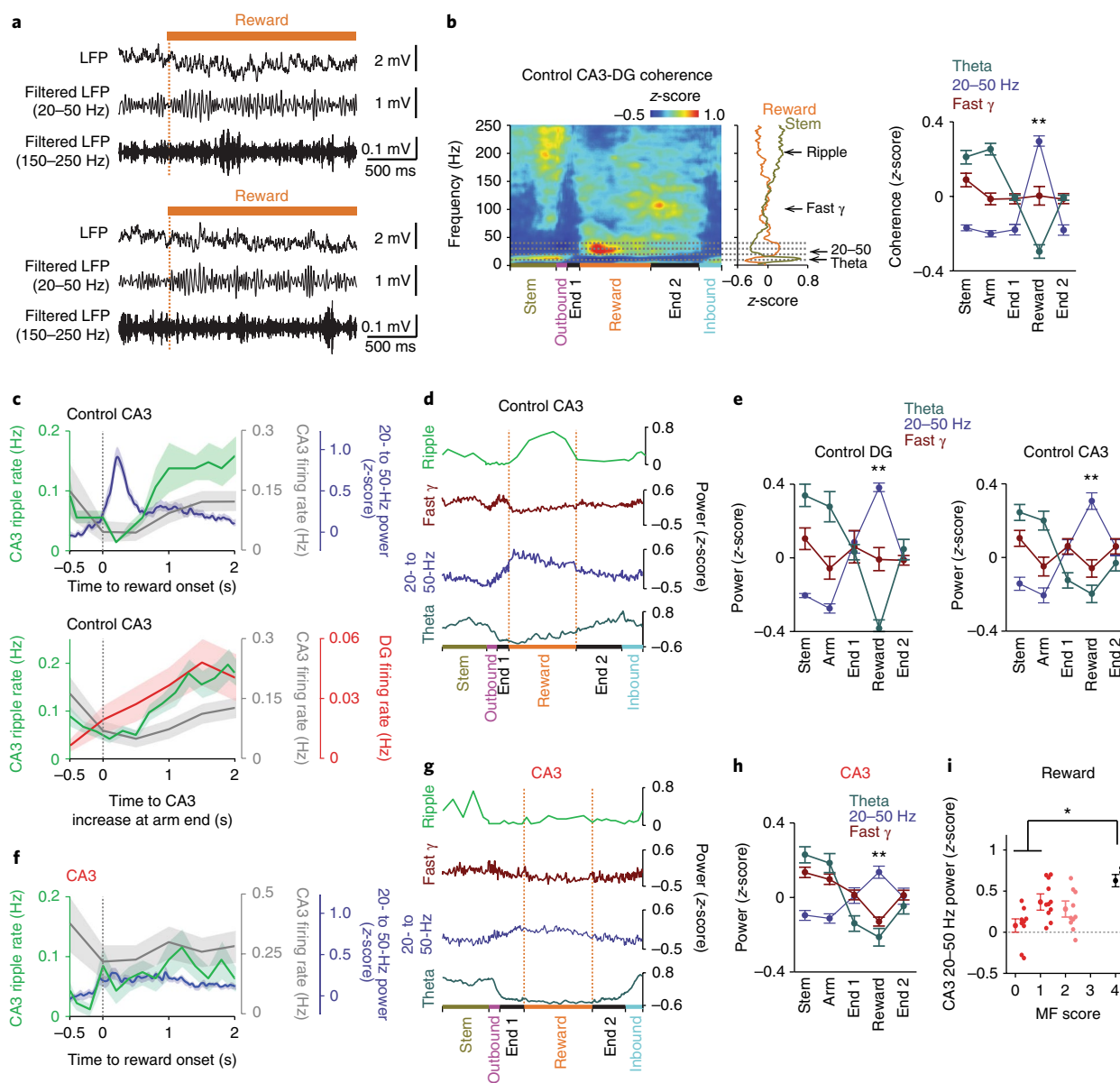
Fig. 5 | CA3 oscillations and DG–CA3 coherence in the 20- to 50-Hz range during reward consumption were dependent on MF input from DG to CA3.
a, Two typical unfiltered and bandpass-filtered (20- to 50-Hz and 150- to 250-Hz) LFP traces aligned to the onset of reward consumption (dashed line).
b, DG–CA3 LFP coherence in a control animal. The average across all trials within a recording day is shown. DG–CA3 coherence in the 20- to 50-Hz range increased during reward, as indicated by asterisks, and coherence in the theta range decreased during reward compared to stem and arm ($n = 35$ tetrode pairs from 4 control animals; theta: $F_{4, 136} = 64.4$, $P < 10^{-10}$, 20–50 Hz: $F_{4, 136} = 307.5$, $P < 10^{-10}$, fast gamma: $F_{4, 136} = 8.7$, $P < 10^{-10}$, repeated-measures ANOVA; increase at reward vs. all the other periods, $**P < 0.01$, Scheffé test). **c**, Time-course of reward-related LFP and single-unit activity in DG and CA3. Top: CA3 ripple events (green, $n = 17$ tetrodes from 4 animals), CA3 20- to 50-Hz power (blue, $n = 17$ tetrodes from 4 animals) and firing rate of CA3 cells (gray, $n = 116$ cells from 4 animals) aligned to the onset of reward consumption. At reward onset, 20- to 50-Hz activity increased whereas ripple event rate and CA3 firing rate was lowest. Bottom: CA3 ripple events (green, $n = 17$ tetrodes from 4 animals) and firing rates of CA3 cells (gray, $n = 116$ from 4 animals) and dentate cells (red, $n = 16$ from 2 animals) are aligned to the onset of the increase in CA3 20- to 50-Hz power. Shaded areas are s.e.m.
d, Behavior-related CA3 ripple event rates and CA3 LFP power in the theta, 20- to 50-Hz and fast-gamma bands across different behavioral periods. **e**, Average LFP power at individual frequency bands in control DG recordings ($n = 8$ tetrodes from 3 animals) and CA3 recordings ($n = 17$ tetrodes from 4 animals). Twenty- to 50-Hz power in DG and CA3 was increased while theta power was decreased during reward consumption (DG: theta: $F_{4,28} = 26.6$, $P < 10^{-10}$, 20–50 Hz: $F_{4,28} = 56.6$, $P < 10^{-10}$, fast gamma: $F_{4,28} = 1.1$, $P = 0.38$; CA3: theta: $F_{4,64} = 13.1$, $P < 10^{-10}$, 20–50 Hz: $F_{4,64} = 22.7$, $P < 10^{-10}$, fast gamma: $F_{4,64} = 2.4$, $P = 0.062$, repeated-measures ANOVA; increase at reward vs. all the other periods, $**P < 0.01$, Scheffé test). **f**, As in **c**, top, but for LMF group (ripple events and 20- to 50-Hz power, $n = 20$ tetrodes from 9 animals; firing rate of CA3 cells, $n = 57$ cells from 9 animals). **g**, As in **d** but for LMF group. **h**, As in **e**, right, but for LMF group ($n = 20$ tetrodes from 9 animals; theta: $F_{4,76} = 29.5$, $P < 10^{-10}$, 20–50 Hz: $F_{4,76} = 20.5$, $P < 10^{-10}$, fast gamma: $F_{4,76} = 30.3$, $P < 10^{-10}$, repeated-measures ANOVA; increase at reward vs. all other periods, $**P < 0.01$, Scheffé test). Error bars are s.e.m. **i**, CA3 20- to 50-Hz power for CA3 recording sites (mean ± s.e.m.; dots correspond to individual sites, grouped by MF score). Reward-associated 20- to 50-Hz power was significantly reduced at CA3 sites with reduced MF input compared to control CA3 sites ($n = 9$, 11, 10 and 17 from 6, 6, 5 and 4 animals for scores 0, 1, 2 and 4, respectively; control vs. HMF, $U = 288$, $Z = 2.49$, $P = 0.26$; control vs. LMF, $U = 431$, $Z = 3.28$, $P = 2.0 \times 10^{-4}$, two-sided Mann–Whitney U test followed by post hoc Bonferroni corrections). $*P < 0.05$, comparison across groups. Error bars are s.e.m.

20- to 50-Hz oscillations and SWRs occurred mostly during separate phases of reward consumption. A transient bout of 20- to 50-Hz oscillations occurred during the first ~0.5 s after the reward encounter, while the incidence of SWRs began to increase after 0.5 s and was highest ~1–2 s after the first contact with the reward (Fig. 5a,c). Furthermore, the two types of oscillations were related to DG and CA3 firing rates in opposite directions (Fig. 5c). DG and CA3 firing rates were low during 20- to 50-Hz oscillations and then gradually increased with increasing SWR occurrence.

Dentate network activity was necessary for reward-associated increases in CA3 firing. The finding that dentate activity and CA3 SWR rates gradually increased at reward locations and that MF inputs to CA3 were required for SWR generation suggested that DG inputs may contribute to spatial WM by modulating CA3 neuronal activity patterns at reward locations. We therefore focused on further examining CA3 network activity and its dependence on DG MF inputs. An increase in CA3 pyramidal cell firing during reward-related SWRs was found for control but not for LMF sites (control vs. LMF, medians: 242% vs. 46%, $U = 3624$, $Z = 2.37$, $P = 0.018$, Mann–Whitney U test; Supplementary Fig. 8c). The lower CA3 firing rates during ripple events, along with the reduced frequency of reward-associated ripples (Fig. 4f), can be expected to jointly result in a prominent reduction in the overall number of CA3 spikes at CA3 sites without MF inputs. Taken together, direct MF inputs from DG granule cells are thus necessary for the generation of reward-associated increases in CA3 SWRs and neuronal firing rates.

The dentate-dependent increase in CA3 SWRs was memory related. We next asked whether the increase in CA3 SWRs was invariably related to reward consumption or may be modulated by WM processing in association with reward consumption, as would be suggested by the finding that effects of DG lesions are particularly pronounced in complex spatial WM tasks[1] and by our finding that SWR rates are particularly high during correct trials. To address this question, we performed recordings on the linear track, where rats retrieved rewards without needing to use spatial memory (Supplementary Fig. 13). On the linear track, SWR dynamics did not differ between LMF, HMF and control sites (Supplementary Fig. 13i). These findings suggest that only memory-related SWR increase is dentate dependent.

Spatial firing patterns of CA3 cells were compromised by DG lesions. After identifying a substantial effect of DG inputs on reward-associated CA3 firing in WM, we next examined whether MF projections also contributed to spatial firing patterns of CA3 place cells ($n = 116$ control, 49 HMF and 57 LMF cells; Fig. 6) and to the relation between spatial and reward-related firing (Fig. 7, and see Supplementary Fig. 14 for additional examples). We first examined how many active CA3 cells we could identify at each of the recording sites. At LMF sites, the number of active cells per tetrode was significantly lower than in controls (range and median for control sites: 2–13 cells and 6 cells; HMF sites: 0–9 cells and 6 cells; LMF sites: 0–7 cells and 2 cells; control vs. HMF: $U = 250.5$, $Z = 0.61$, $P > 0.99$; control vs. LMF: $U = 443.5$, $Z = 3.70$, $P = 4.2 \times 10^{-4}$, Mann–Whitney U test followed by post hoc Bonferroni corrections; Fig. 6b), but the firing rates of each of the recorded cells were significantly higher than in controls (range and median for control sites: 0.00–1.21 Hz and 0.07 Hz; HMF sites: 0.00–3.14 Hz and 0.16 Hz; LMF sites: 0.00–2.88 Hz and 0.19 Hz; control vs. LMF: $D_{max} = 0.30$, $P = 0.0024$; control vs. HMF: $D_{max} = 0.20$; $P = 0.11$, Kolmogorov–Smirnov test; Fig. 6c). The lesion data suggest that the removal of MF inputs to CA3 altered CA3 network sparsity and excitability such that fewer CA3 cells were active but with each active cell firing at a higher rate.

We then analyzed the spatial firing patterns of CA3 cells with an average firing rate of >0.05 Hz during the spatial WM task (control,

$n = 64$ cells; HMF, $n = 34$ cells; LMF, $n = 47$ cells). In the control group, 50.0% and 27.8% of active CA3 neurons had a place field on either a single arm or on the stem, respectively. Together, more than 75% of active CA3 cells thus had detectable fields on the maze. Furthermore, recordings in the RF task on the same maze on the same day showed that CA3 place cells had similar spatial maps of the environment between the spatial WM and RF tasks (Supplementary Fig. 3b). Field locations in CA3 were therefore predominantly determined by spatial location rather than by task demands, as previously reported[32]. The spatial firing of control CA3 cells during WM was then compared to cells from DG-lesioned rats during WM. While place fields were generally larger and more dispersed with dentate lesions, the reduced spatial stability of CA3 firing after DG lesions occurred at all CA3 recording sites regardless of the degree of MF reduction (Fig. 6c,d). This differs from the effects on reward-associated CA3 firing, which were directly dependent on the degree of remaining MF inputs to a particular recording site.

Prospective firing of CA3 place cells during reward periods depended on direct input from DG. In awake SWRs, sequences of place-specific neurons are replayed in both prospective and retrospective manners[13–16]. To examine out-of-field reactivation patterns of CA3 cells at the reward locations in the spatial WM task, we selected CA3 cells with place fields preferentially on a single arm of the radial maze (control, $n = 39$ cells; LMF, $n = 22$ cells) and analyzed out-of-field spikes that occurred at reward locations on arms other than the arm with the place field (Fig. 7a,b). We first confirmed that most reward-associated out-of-field spikes occurred in close temporal association with SWRs (Fig. 7c), and then analyzed when these spikes occurred throughout the series of arm entries in each trial. For each cell and each trial, reward-associated spikes before entering the arm with the place field were considered prospective, and spikes after exiting the arm with the field were defined as retrospective (Fig. 7b,d). In the control group, reward-associated prospective CA3 firing rates were significantly higher than retrospective firing rates (prospective: 0.15 ± 0.02 Hz, retrospective: 0.08 ± 0.01 Hz, $t_{38} = 3.57$, $P = 9.8 \times 10^{-4}$, paired t test; Fig. 7f). The higher likelihood for prospective firing is consistent with a tendency for a decrease in reward-associated firing rates over the time throughout a trial (Supplementary Fig. 15a). For quantification of the relative strength of prospective compared to retrospective firing, a ratio between these rates was defined for individual cells (difference divided by the sum). The prospective ratio ranged between −1 and +1, with a higher positive value reporting stronger bias toward prospective firing. The average prospective ratio in the spatial WM task was +0.34 ± 0.07 (Fig. 7f), indicating that firing during reward consumption preferentially included cells with place fields on arms that had not yet been visited within the trial. At LMF recording sites, no difference was observed between reward-associated prospective and retrospective firing rates (prospective: 0.38 ± 0.07 Hz, retrospective: 0.32 ± 0.05 Hz, $t_{21} = 0.97$, $P = 0.34$, paired t test; Fig. 7d,f), and the prospective ratio was significantly lower than in the control group (control: 0.34 ± 0.07, LMF: 0.05 ± 0.08, $t_{59} = 2.60$, $P = 0.012$, Student's t test; Fig. 7f). Similarly, preferential prospective firing in the control but not in the LMF group was also observed when restricting the analysis to only spikes that occurred during SWR events that were detected on the same recording electrode as the spikes (control: prospective, 0.67 ± 0.13 Hz; retrospective, 0.35 ± 0.08 Hz; $t_{38} = 2.15$, $P = 0.038$, paired t test; LMF: prospective, 0.37 ± 0.13 Hz; retrospective, 0.35 ± 0.09 Hz; $t_{21} = 0.70$, $P = 0.49$, paired t test; Fig. 7e,g), but the difference of prospective ratios between the two groups no longer reached significance with the smaller sample size (control: 0.22 ± 0.10, LMF: −0.09 ± 0.13, $t_{59} = 1.86$, $P = 0.068$, t test; Fig. 7g). These results suggest that hippocampal representation of future locations in the spatial WM task occurred during reward periods during the spatial WM task and that the emergence of these reward-related
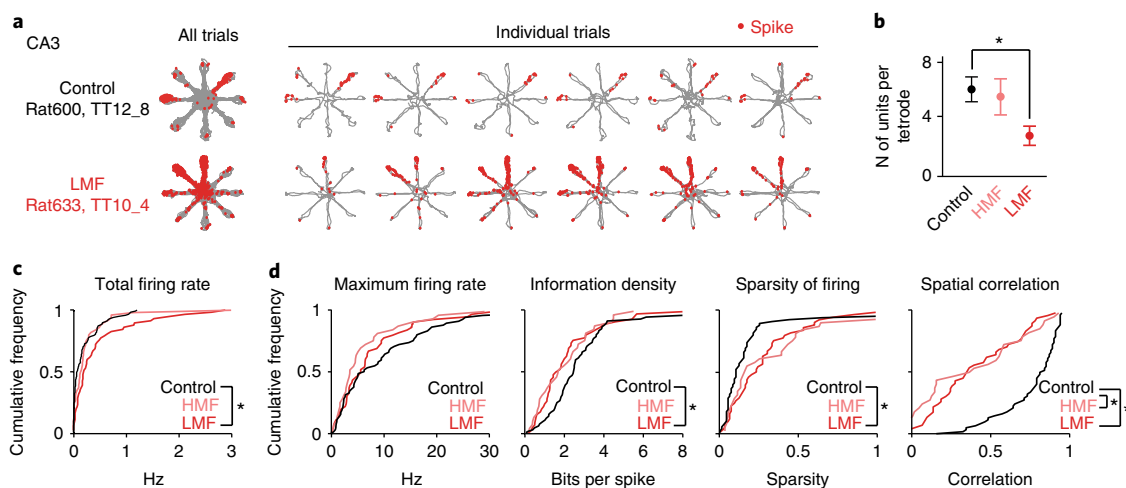
Fig. 6 | Place-specific firing of CA3 pyramidal neurons. a, Each row is a representative example of place-specific firing of a CA3 pyramidal cell (top, control; bottom, DG-lesioned) in the spatial WM task. Similar results were obtained in 116 control cells from 4 rats and in 57 LMF cells from 9 DG-lesioned rats, and they are quantified in panels **c** and **d**. For each neuron, the trajectories (gray) with spike locations (red dots) are shown superimposed for all 20 trials in a recording session and separately for the first 6 trials (from left to right). CA3 place fields in control animals were frequently restricted to a single arm, but firing fields were broader at recording sites of DG-lesioned rats (see Supplementary Fig. 14 for additional examples). **b**, Average number of CA3 principal cells that were recorded from each tetrode. Fewer CA3 neurons were detected at LMF sites than at CA3 recording sites from control rats or at HMF sites from DG-lesioned rats ($n = 17$, 10 and 20 in control, HMF and LMF sites in 4, 5 and 9 animals, respectively; control vs. HMF, $U = 250.5$, $Z = 0.61$, $P > 0.99$; control vs. LMF, $U = 443.5$, $Z = 3.70$, $P = 4.2 \times 10^{-4}$, two-sided Mann–Whitney U test followed by post hoc Bonferroni corrections). *$P < 0.05$. Error bars are s.e.m. **c**, Cumulative distribution of total firing rates for the entire sample of CA3 cells ($n = 116$, 48 and 57 cells from 4, 5 and 9 animals in control, HMF and LMF groups, respectively). The firing rates of CA3 neurons were selectively increased at LMF sites (control vs. HMF, $D_{max} = 0.20$, $P = 0.11$; control vs. LMF, $D_{max} = 0.30$, $P = 0.0024$, Kolmogorov–Smirnov test with Bonferroni's correction). *$P < 0.05$. **d**, Cumulative distribution of maximum in-field firing rates, information density scores, sparsity of firing and spatial correlation for CA3 cells recorded from control, HMF and LMF sites ($n = 64$, 34 and 47 cells from 4, 5 and 9 animals, respectively). Spatial measurements were calculated from all cells with an average firing rate >0.05 Hz. The precision of spatial firing was reduced in DG-lesioned rats, and the effect was more pronounced at LMF sites (maximum firing rate, control vs. HMF, $D_{max} = 0.26$, $P = 0.16$; control vs. LMF, $D_{max} = 0.16$, $P = 0.84$; information density, control vs. HMF, $D_{max} = 0.26$, $P = 0.15$; control vs. LMF, $D_{max} = 0.30$, $P = 0.022$; sparsity, control vs. HMF, $D_{max} = 0.30$, $P = 0.051$; control vs. LMF, $D_{max} = 0.35$, $P = 0.0030$). However, reliability of spatial firing was reduced irrespective of MF density (spatial correlation, control vs. HMF, $D_{max} = 0.56$, $P = 3.2 \times 10^{-6}$; control vs. LMF, $D_{max} = 0.55$, *$P = 1.4 \times 10^{-7}$, Kolmogorov–Smirnov test with Bonferroni's correction). *$P < 0.05$.

firing patterns in the CA3 circuit is supported by direct MF inputs from dentate granule neurons.

If the SWRs and the associated prospective neuronal signals support the planning of future trajectories, these activity patterns should be relevant to behavioral performance[33]. Accordingly, prospective firing at control recording sites was observed on correct trials but not incorrect trials (Supplementary Fig. 16). Notably, prospective firing also emerged at LMF sites during correct but not incorrect trials (correct: prospective, 0.43 ± 0.08 Hz; retrospective, 0.26 ± 0.04 Hz; $t_{20} = 2.80$, $P = 0.011$; incorrect: prospective, 0.37 ± 0.08 Hz; retrospective, 0.35 ± 0.07 Hz; $t_{20} = 0.31$, $P = 0.76$, paired t test; Supplementary Fig. 16d). These results suggest that prospective neuronal signals predict successful behavioral performance and that even CA3 networks with only minor remaining DG inputs generate prospective coding on occasions when animals are more likely to make correct decisions. While we found that additional firing patterns of CA3 cells, such as phase-locking to theta and gamma oscillations, were also reduced by DG lesions, we did not find that phase-locking differed between correct and incorrect trials in either lesioned or control rats (Supplementary Fig. 17), which suggests that these effects are less directly related to ongoing WM performance.

Discussion

The DG is the first processing stage in the hippocampal trisynaptic circuit, and its contribution to intrahippocampal processing is thought to be particularly critical when two or more closely related items need to be retained in memory. Previous studies have

therefore investigated the ability of dentate cells to separate similar input patterns by generating distinct patterns of neuronal activity, with a particular focus on pattern separation by distinct spatial firing patterns[2,3]. However, complex spatial WM tasks have been found to require not only dentate granule neurons[34] but also hippocampal SWRs[21], and we therefore asked whether the role of the dentate cells in memory may extend beyond pattern separation. We began by confirming that selective lesions of the dentate gyrus impaired spatial WM, and then used the same task for recording neural activity in intact and DG-lesioned rats. While we found standard place fields for a subset of dentate cells, as previously reported, we also identified a large proportion of cells with very low average firing rates (< 0.1 Hz). In standard spatial analysis these cells would be considered silent[35,36], but they consistently fired at one or more reward locations. The increased firing of dentate cells at reward locations was preceded by a brief 20- to 50-Hz oscillation and occurred in parallel with an increase in CA3 SWR and neuronal activity. Furthermore, it was predominantly CA3 cells with place fields on not-yet-visited arms that were active on the arm ends over the course of each trial. Lesions of dentate granule neurons precluded the increase of CA3 SWRs and of prospective CA3 neuronal activity at the reward site. Taken together, these findings reveal a role of dentate computations beyond pattern separation and suggest that the dentate gyrus is necessary for the generation of neuronal firing patterns that support goal-directed behavior.

Previously undescribed type of nonspatial firing of dentate granule cells. The focus of previous work has been on spatial firing
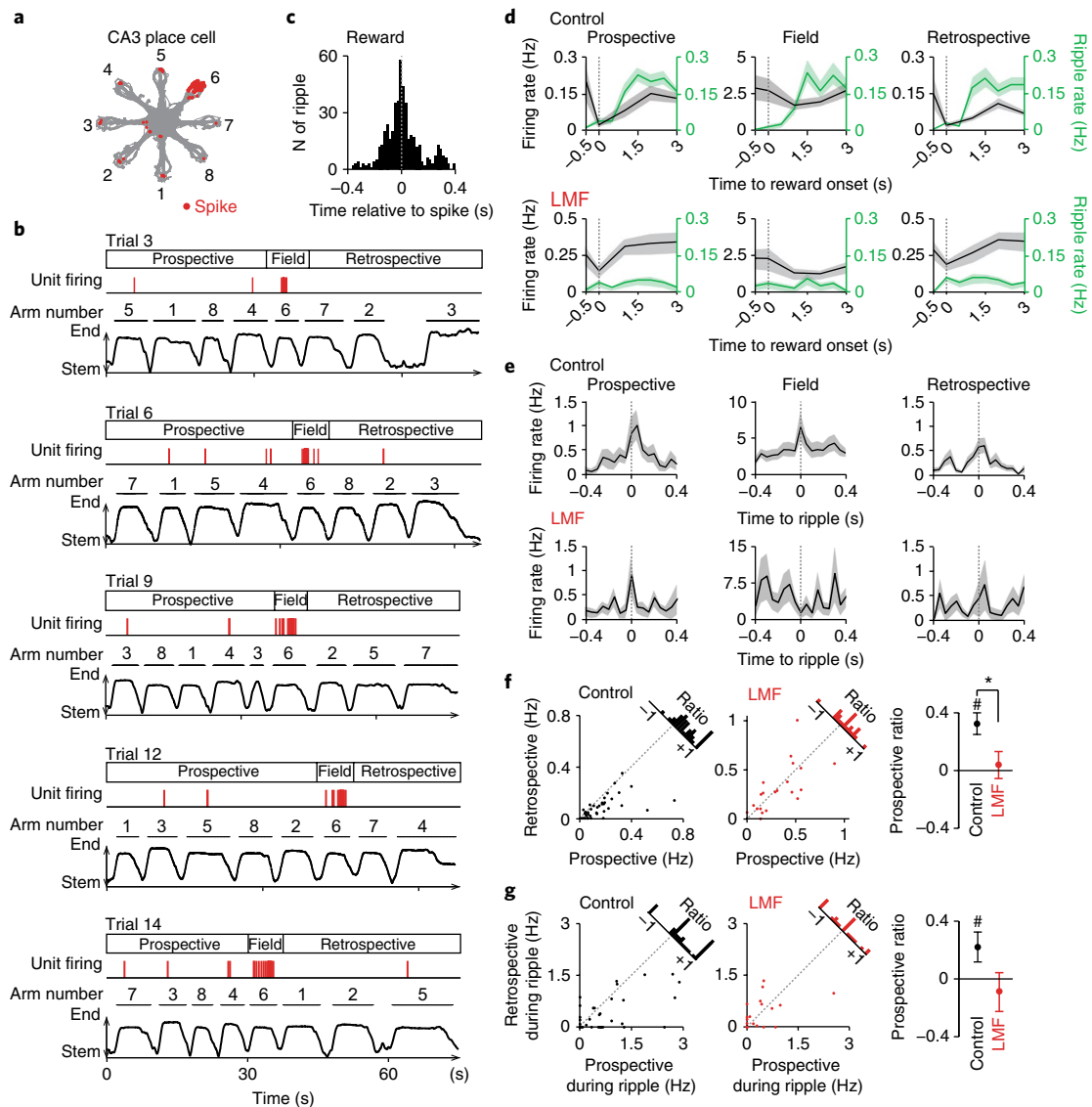
Fig. 7 | Prospective firing of CA3 neurons during SWRs was dependent on direct MF innervation from DG. a, Spatial firing pattern of a representative CA3 neuron. Trajectories (gray) with spike locations (red dots) are superimposed for 20 trials of the WM task. The firing of the CA3 neuron was highest within the place field on arm 6, but spiking also occurred during ripples at reward locations. Similar place fields with firing predominantly on one maze arm were found and analyzed for 39 control CA3 cells from 4 animals and 22 cells at LMF sites in 6 DG-lesioned animals. **b**, Example trials show spiking within the field and at reward locations for the same cell as in **a**. Top of each panel: spike times are shown as red ticks. Bottom of each panel: the behavioral timeline is indicated by the distance from the maze center. Prospective and retrospective firing was defined as the reward-related firing before and after the animal entered the arm with the cell's place field. **c**, Cross-correlogram of spikes with CA3 ripples, demonstrating that spikes mostly occurred in close temporal association with SWR events. **d**, Reward-associated firing rates of CA3 cells for arm entries before (prospective), during (field) and after (retrospective) visiting the arm with the place field. There was a significant difference between prospective and retrospective CA3 firing (gray) during reward consumption (0–3 s after the reward onset) at control sites ($n = 39$ cells from 4 animals, prospective vs. retrospective, $F_{1, 228} = 6.04$, $P = 0.016$, repeated-measures ANOVA) but not LMF sites ($n = 22$ cells from 6 animals, $F_{1, 126} = 0$, $P = 0.99$). Corresponding ripple event rates (green) are superimposed on the same graph. While control prospective and retrospective CA3 firing rates differed, we found no change in the ripple rate between prospective and retrospective periods (prospective vs. retrospective, control: $F_{1, 456} = 0.21$, $P = 0.65$; LMF: $F_{1, 252} = 0.04$, $P = 0.85$, repeated-measures ANOVA). Lines with shaded regions are mean ± s.e.m. **e**, CA3 ripple-triggered firing rate changes. There was a significant difference between prospective and retrospective CA3 firing during ripples (0–150 ms after the ripple onset) in the control group (prospective vs. retrospective, $F_{1, 228} = 4.64$, $P = 0.034$, repeated-measures ANOVA) but not LMF group ($F_{1, 126} = 0.02$, $P = 0.89$). Lines with shaded regions are mean ± s.e.m. **f**, Left: for all CA3 cells, prospective and retrospective firing rates are plotted for spikes during reward (control neurons, black dots; neurons at LMF sites, red dots). Many control cells are below the identity line, which indicates higher prospective than retrospective firing (prospective vs. retrospective, $t_{38} = 3.57$, $P = 9.8 \times 10^{-4}$, two-sided paired t test). In contrast, the cells from LMF sites scatter around the identity line and do not show a systematic preference ($t_{21} = 0.97$, $P = 0.34$). Right: the prospective ratio (i.e., prospective firing rate divided by retrospective firing rate) decreased selectively for CA3 neurons with LMF input (control vs. LMF, $t_{59} = 2.60$, $P = 0.012$; comparison from zero, control: $t_{38} = 5.09$, $P = 1.0 \times 10^{-5}$, two-sided paired t test; LMF: $t_{21} = 0.57$, $P = 0.57$). #$P < 0.05$, comparison from zero within the group; *$P < 0.05$, comparison across the groups. **g**, As in **f** but for the prospective ratio of CA3 firing during reward-associated ripple events (prospective vs. retrospective, control: $t_{38} = 2.15$, $P = 0.0077$, two-sided paired t test; LMF: $t_{21} = 0.13$, $P = 0.89$; prospective ratio control vs. LMF, $t_{59} = 1.86$, $P = 0.068$; prospective ratio compared from zero, control: $t_{38} = 2.15$, $P = 0.038$, two-sided paired t test; LMF: $t_{21} = 0.70$, $P = 0.49$). #$P < 0.05$.

patterns of dentate cells and proposed a role in pattern separation of these firing patterns, with the suggestion that multipeaked spatial cells are particularly well suited to discriminate between input patterns[2,3,37]. Recently, multipeaked spatial firing patterns were found to be typical for hilar mossy cells, while dentate granule cells had either single fields or were silent during behavior[25–27]. Our analysis of firing patterns of dentate cells is consistent with these results, but also identifies another role for sparsely active dentate granule cells (~65%) that would be considered silent in standard spatial analysis. We found that these cells could become selectively active at the arm ends during reward consumption. For many of these cells, the activity was not at a single reward location in the maze, but rather at multiple reward locations over a series of trials, and the same cells rarely had standard place fields on the maze. In addition, detailed analysis of the behavioral pattern at the reward location revealed that dentate activity at the reward location peaked about 0.5–1 s after the reward consumption commenced. Together with the spatial WM deficits after selective dentate granule cell lesions, these findings therefore suggest that the activity of a large proportion of dentate cells after the onset of reward consumption is necessary for spatial WM computations. These computations could include the tagging of the current reward location as a no longer valid target or the selection of a not-yet-visited location on the maze as the next target.

20- to 50-Hz oscillations at the onset of the reward period. Because we hypothesized that the updating of spatial WM is a computation that could be performed by circuits that include loops between the DG and the hippocampal CA3 region, we asked whether the dentate activity during the reward period was associated with oscillatory patterns and increased neuronal activity in CA3. While we found a striking increase in both 20- to 50-Hz oscillations as well as in SWRs during reward consumption, we found that these oscillatory events were largely non-overlapping. Immediately after reward encounter, a brief (<0.5 s) bout of pronounced 20- to 50-Hz oscillations emerged, while the incidence of SWRs peaked during the later period of reward consumption in parallel with the increase in dentate firing.

Oscillation frequencies between 20- to 50-Hz include frequency bands that have been previously referred to as slow gamma, 20- to 40-Hz and beta oscillations[38]. However, the occurrence of reward-related 20- to 50-Hz oscillations in CA3 while neuronal activity is low would preclude these oscillations from directly corresponding to either 20- to 40-Hz oscillations or slow gamma, which have been reported selectively in CA1 or along with CA3 activation, respectively[39–43]. Even though beta oscillations in the dentate subregion have previously been described as evoked by cue encounters[44,45], our 20- to 50-Hz oscillations at reward were much more prominent in the spatial WM task compared to the linear track. If our oscillations were therefore of a similar mechanistic origin as cue-related beta oscillations, they would have been substantially amplified by memory processing.

Furthermore, none of the previous studies examined the lack of entrainment of either the DG or CA3 networks that we found here, and our reward-related 20- to 50-Hz oscillations in DG and CA3 occurred while firing rates in both neuronal populations were at a minimum. The finding that these oscillations were nonetheless DG-dependent raises the possibility that the oscillations predominantly reflect synaptic currents that are evoked by afferent inputs to the DG–CA3 network or by afferent inputs to the DG and volume conduction to CA3, which would be diminished by degeneration of the target cell population. An additional possibility is that the DG lesion precluded the activation of local interneurons that coordinate the synchrony of the oscillations between the DG and CA3 dendritic regions.

Dentate granule neuron activity was necessary for increased CA3 firing and sharp wave ripple generation during reward consumption. The parallel increase of dentate activity, CA3 activity and CA3 SWRs following the initial contact with the reward, along with the strong inputs from DG to CA3, suggested that DG inputs were required for activating CA3 during reward-associated immobility. We directly tested this prediction by performing lesions of the DG granule cells and found a substantial attenuation of the increase in CA3 SWRs during the period of contact with the reward. Notably, DG lesions did not result in a general decrease of CA3 activity, but rather resulted in an elevated average firing rate of CA3 cells during theta periods, as previously reported[46]. While this may be a compensatory response that could also result in larger CA3 fields, the inputs from DG to CA3 were specifically required for eliciting brief bouts of CA3 SWRs after reward encounter in the spatial WM task, while DG-lesion effects were not observed on the linear track. These results suggest that DG is specifically required for a memory-related elevation in CA3 activity. In addition, the difference between the WM results and the linear track results is consistent with the possibility that there are both dentate-dependent and dentate-independent SWRs in CA3, as previously reported in slice experiments[47].

DG participated in biasing arm-end CA3 activity toward not-yet-visited spatial locations. Given that CA3 neuronal activity and CA3 SWRs were selectively increased throughout reward consumption, we examined whether reward-related neuronal activity may be informative for successfully completing the spatial WM task. As each trial progressed, CA3 cells with place fields on not-yet-visited arms fired preferentially during reward consumption, as if CA3 performed a look-ahead toward possible future target locations. Consistent with the suggestion that such prospective coding may be necessary for guiding future choices, we found that look-ahead CA3 activity was more pronounced during correct trials than in incorrect trials and that the WM deficits after DG lesions were accompanied by a loss of prospective coding. DG lesions therefore not only attenuated the emergence of SWRs at the arm ends but also, concurrently, reduced the information content of the remaining SWRs. We also note that prospective coding tended to reemerge in correct trials in DG-lesioned rats. Remaining MF inputs to CA3 were, in the many incorrect trials, thus not sufficient for generating prospective coding. However, when prospective coding was occasionally generated, its occurrence was associated with a higher likelihood for a trial to be completed correctly.

The relation between spatial WM performance and representing future locations during reward consumption raises the question of how neuronal activity that points to future locations could subsequently result in the realization of successful movement sequences. This type of progression has been implemented for theta sequences in computational models[7], and recent experimental work has shown that the information contents of SWRs and theta sequences are related[48]. We therefore hypothesize that intrahippocampal networks can generate continuity between theta and nontheta states, allowing for preferential prospective activity during CA3 SWRs to contribute to the selection of particular theta sequences. The selection could either be mediated by a strong feedforward signal from dentate to CA3 or by loops that engage the associational projections from CA3 back to DG. Irrespective of how the computation is implemented in the DG–CA3 network, our data show that the DG and, in particular, the nonspatial DG firing patterns after contact with the reward, are a critical component of neuronal computations that support spatial WM. Taken together, we found a new type of firing pattern of otherwise silent dentate neurons and show that DG supports an increase in CA3 SWRs and CA3 prospective activity patterns during the period after contact with the reward, suggesting a role for dentate activity in SWR generation and goal

selection. Computations of the dentate gyrus are thus not limited to pattern separation, but are also more directly involved in organizing memory-guided behavior.

Methods

Methods, including statements of data availability and any associated accession codes and references, are available at https://doi.org/10.1038/s41593-017-0061-5.

References

1. Xavier, G. F. & Costa, V. C. Dentate gyrus and spatial behaviour. *Prog. Neuropsychopharmacol. Biol. Psychiatry* **33**, 762–773 (2009).
2. Leutgeb, J. K., Leutgeb, S., Moser, M. B. & Moser, E. I. Pattern separation in the dentate gyrus and CA3 of the hippocampus. *Science* **315**, 961–966 (2007).
3. Neunuebel, J. P. & Knierim, J. J. CA3 retrieves coherent representations from degraded input: direct evidence for CA3 pattern completion and dentate gyrus pattern separation. *Neuron* **81**, 416–427 (2014).
4. Amaral, D. G. & Witter, M. P. The three-dimensional organization of the hippocampal formation: a review of anatomical data. *Neuroscience* **31**, 571–591 (1989).
5. Scharfman, H. E. The CA3 "backprojection" to the dentate gyrus. *Prog. Brain Res.* **163**, 627–637 (2007).
6. Treves, A. & Rolls, E. T. Computational analysis of the role of the hippocampus in memory. *Hippocampus* **4**, 374–391 (1994).
7. Lisman, J. E., Talamini, L. M. & Raffone, A. Recall of memory sequences by interaction of the dentate and CA3: a revised model of the phase precession. *Neural Netw.* **18**, 1191–1201 (2005).
8. Buzsáki, G. Hippocampal sharp waves: their origin and significance. *Brain Res.* **398**, 242–252 (1986).
9. Csicsvari, J., Hirase, H., Mamiya, A. & Buzsáki, G. Ensemble patterns of hippocampal CA3-CA1 neurons during sharp wave-associated population events. *Neuron* **28**, 585–594 (2000).
10. Oliva, A., Fernández-Ruiz, A., Buzsáki, G. & Berényi, A. Role of hippocampal CA2 region in triggering sharp-wave ripples. *Neuron* **91**, 1342–1355 (2016).
11. Buzsáki, G., Horváth, Z., Urioste, R., Hetke, J. & Wise, K. High-frequency network oscillation in the hippocampus. *Science* **256**, 1025–1027 (1992).
12. Lee, A. K. & Wilson, M. A. Memory of sequential experience in the hippocampus during slow wave sleep. *Neuron* **36**, 1183–1194 (2002).
13. Foster, D. J. & Wilson, M. A. Reverse replay of behavioural sequences in hippocampal place cells during the awake state. *Nature* **440**, 680–683 (2006).
14. Pfeiffer, B. E. & Foster, D. J. Hippocampal place-cell sequences depict future paths to remembered goals. *Nature* **497**, 74–79 (2013).
15. Diba, K. & Buzsáki, G. Forward and reverse hippocampal place-cell sequences during ripples. *Nat. Neurosci.* **10**, 1241–1242 (2007).
16. Karlsson, M. P. & Frank, L. M. Awake replay of remote experiences in the hippocampus. *Nat. Neurosci.* **12**, 913–918 (2009).
17. Carr, M. F., Jadhav, S. P. & Frank, L. M. Hippocampal replay in the awake state: a potential substrate for memory consolidation and retrieval. *Nat. Neurosci.* **14**, 147–153 (2011).
18. Dupret, D., O'Neill, J., Pleydell-Bouverie, B. & Csicsvari, J. The reorganization and reactivation of hippocampal maps predict spatial memory performance. *Nat. Neurosci.* **13**, 995–1002 (2010).
19. Ego-Stengel, V. & Wilson, M. A. Disruption of ripple-associated hippocampal activity during rest impairs spatial learning in the rat. *Hippocampus* **20**, 1–10 (2010).
20. Girardeau, G., Benchenane, K., Wiener, S. I., Buzsáki, G. & Zugaro, M. B. Selective suppression of hippocampal ripples impairs spatial memory. *Nat. Neurosci.* **12**, 1222–1223 (2009).
21. Jadhav, S. P., Kemere, C., German, P. W. & Frank, L. M. Awake hippocampal sharp-wave ripples support spatial memory. *Science* **336**, 1454–1458 (2012).
22. Sullivan, D. et al. Relationships between hippocampal sharp waves, ripples, and fast gamma oscillation: influence of dentate and entorhinal cortical activity. *J. Neurosci.* **31**, 8605–8616 (2011).
23. Penttonen, M., Kamondi, A., Sik, A., Acsády, L. & Buzsáki, G. Feed-forward and feed-back activation of the dentate gyrus in vivo during dentate spikes and sharp wave bursts. *Hippocampus* **7**, 437–450 (1997).
24. Bragin, A., Jandó, G., Nádasdy, Z., van Landeghem, M. & Buzsáki, G. Dentate EEG spikes and associated interneuronal population bursts in the hippocampal hilar region of the rat. *J. Neurophysiol.* **73**, 1691–1705 (1995).
25. Senzai, Y. & Buzsáki, G. Physiological properties and behavioral correlates of hippocampal granule cells and mossy cells. *Neuron* **93**, 691–704.e5 (2017).
26. Danielson, N. B. et al. In vivo imaging of dentate gyrus mossy cells in behaving mice. *Neuron* **93**, 552–559.e4 (2017).
27. GoodSmith, D. et al. Spatial representations of granule cells and mossy cells of the dentate gyrus. *Neuron* **93**, 677–690.e5 (2017).
28. O'Neill, J., Senior, T. & Csicsvari, J. Place-selective firing of CA1 pyramidal cells during sharp wave/ripple network patterns in exploratory behavior. *Neuron* **49**, 143–155 (2006).
29. Buzsáki, G. Hippocampal sharp wave-ripple: A cognitive biomarker for episodic memory and planning. *Hippocampus* **25**, 1073–1188 (2015).
30. Kay, K. et al. A hippocampal network for spatial coding during immobility and sleep. *Nature* **531**, 185–190 (2016).
31. Ahmed, O. J. & Mehta, M. R. Running speed alters the frequency of hippocampal gamma oscillations. *J. Neurosci.* **32**, 7373–7383 (2012).
32. Leutgeb, S. & Leutgeb, J. K. Pattern separation, pattern completion, and new neuronal codes within a continuous CA3 map. *Learn. Mem.* **14**, 745–757 (2007).
33. Singer, A. C., Carr, M. F., Karlsson, M. P. & Frank, L. M. Hippocampal SWR activity predicts correct decisions during the initial learning of an alternation task. *Neuron* **77**, 1163–1173 (2013).
34. McLamb, R. L., Mundy, W. R. & Tilson, H. A. Intradentate colchicine disrupts the acquisition and performance of a working memory task in the radial arm maze. *Neurotoxicology* **9**, 521–528 (1988).
35. Jung, M. W. & McNaughton, B. L. Spatial selectivity of unit activity in the hippocampal granular layer. *Hippocampus* **3**, 165–182 (1993).
36. Neunuebel, J. P. & Knierim, J. J. Spatial firing correlates of physiologically distinct cell types of the rat dentate gyrus. *J. Neurosci.* **32**, 3848–3858 (2012).
37. Myers, C. E. & Scharfman, H. E. Pattern separation in the dentate gyrus: a role for the CA3 backprojection. *Hippocampus* **21**, 1190–1215 (2011).
38. Colgin, L. L. Do slow and fast gamma rhythms correspond to distinct functional states in the hippocampal network? *Brain Res.* **1621**, 309–315 (2015).
39. Atallah, B. V. & Scanziani, M. Instantaneous modulation of gamma oscillation frequency by balancing excitation with inhibition. *Neuron* **62**, 566–577 (2009).
40. Tort, A. B., Komorowski, R. W., Manns, J. R., Kopell, N. J. & Eichenbaum, H. Theta-gamma coupling increases during the learning of item-context associations. *Proc. Natl Acad. Sci. USA* **106**, 20942–20947 (2009).
41. Carr, M. F., Karlsson, M. P. & Frank, L. M. Transient slow gamma synchrony underlies hippocampal memory replay. *Neuron* **75**, 700–713 (2012).
42. Hsiao, Y. T., Zheng, C. & Colgin, L. L. Slow gamma rhythms in CA3 are entrained by slow gamma activity in the dentate gyrus. *J. Neurophysiol.* **116**, 2594–2603 (2016).
43. Igarashi, K. M., Lu, L., Colgin, L. L., Moser, M. B. & Moser, E. I. Coordination of entorhinal-hippocampal ensemble activity during associative learning. *Nature* **510**, 143–147 (2014).
44. Martin, C., Beshel, J. & Kay, L. M. An olfacto-hippocampal network is dynamically involved in odor-discrimination learning. *J. Neurophysiol.* **98**, 2196–2205 (2007).
45. Rangel, L. M., Chiba, A. A. & Quinn, L. K. Theta and beta oscillatory dynamics in the dentate gyrus reveal a shift in network processing state during cue encounters. *Front. Syst. Neurosci.* **9**, 96 (2015).
46. McNaughton, B. L., Barnes, C. A., Meltzer, J. & Sutherland, R. J. Hippocampal granule cells are necessary for normal spatial learning but not for spatially-selective pyramidal cell discharge. *Exp. Brain Res.* **76**, 485–496 (1989).
47. Hofer, K. T. et al. The hippocampal CA3 region can generate two distinct types of sharp wave-ripple complexes, in vitro. *Hippocampus* **25**, 169–186 (2015).
48. Pfeiffer, B. E. & Foster, D. J. Place cells. Autoassociative dynamics in the generation of sequences of hippocampal place cells. *Science* **349**, 180–183 (2015).

Author contributions

T.S., V.C.P., S.L. and J.K.L. designed experiments. V.C.P developed the lesion and performed the behavioral testing and dentate electrophysiological recording experiments. S.A. performed preliminary analyses of dentate recordings. T.S. performed

CA3 electrophysiological recordings and behavior in DG-lesioned animals, with assistance from E.H. with behavior, histology and microscopy. T.S. performed all reported analyses. J.E.L. provided conceptual discussions. T.S., S.L. and J.K.L. wrote the manuscript.

Competing interests

The authors declare no competing financial interests.

Additional information

Supplementary information is available for this paper at https://doi.org/10.1038/s41593-017-0061-5.

Reprints and permissions information is available at www.nature.com/reprints.

Correspondence and requests for materials should be addressed to J.K.L.

Publisher's note: Springer Nature remains neutral with regard to jurisdictional claims in published maps and institutional affiliations.

Methods

Approvals. All surgical and experimental procedures were approved by the Institutional Animal Care and Use Committee at the University of California, San Diego, and conducted at the University of California, San Diego according to National Institutes of Health guidelines.

Subjects. A total of 37 male Long Evans rats (3–6 months old) were used in this study. The animals were housed individually and maintained on a 12-h light/12-h dark schedule with lights off at 6:00 a.m. All animals were obtained from Charles River Laboratory. Following at least 1 week of adaptation to the laboratory, access to food was restricted and the rats were maintained at about 85% of free-feeding body weight. Water was readily available.

Sixteen animals were trained in a spatial working memory (WM) task and used for behavioral testing before and after either a dentate lesion ($n = 11$) or sham surgery ($n = 5$). Twenty animals were used for recordings in the WM task. Ten of these animals received a surgery during which a chronic electrophysiological recording assembly was implanted, and 10 animals received both an implant and a dentate lesion. On days with recordings, 16 animals (7 control and 9 lesioned) first performed the WM task and next performed a random foraging (RF) task. Four animals performed only the WM task. After recordings in the WM task for at least 3 d, six recording animals (three control and three lesioned) performed a linear track task. One additional animal with a recording assembly and dentate lesion performed only the linear track task. Control and lesioned animals from the same litters were assigned randomly and tested experimentally in parallel.

Spatial WM task on the radial eight-arm maze. All behavioral training occurred in the rats' dark phase. Rats were trained on a semiautomated black Plexiglas eight-arm radial maze with a central circular platform (27 cm diameter) and eight arms (79 cm × 12 cm) to which access was controlled by a remote switch. First, daily 10-min habituation sessions with immediate access to all eight arms were performed until the rat ate the chocolate milk reward (0.2 mL) at the end of each arm. In the next training stage, each trial started with access to all arms initially restricted. After an interval of 2 min, the experimenter made the first arm available and then sequentially presented one arm at a time up to the fourth arm (forced phase). The sequences during the forced phase were pseudorandom, excluding instances in which all four arms would have been presented in spatial order (i.e., 1, 2, 3, 4). Immediately after the forced phase, all eight arms were presented simultaneously (choice phase). During the choice phase, the animal was expected to visit the remaining four baited arms, and reentries into previously visited arms were considered errors. A trial ended when the rat had retrieved the reward from all eight arms and returned to the central platform, or if the total time exceeded 10 min. When a trial was stopped for exceeding the time limit, it was removed from analysis. After an intertrial interval of 2 min, the next trial was initiated. Each day the rat was trained to perform 6–10 trials within 30 min a day and training was continued until the percentage of correct trials (i.e., trials without any errors) over 5 consecutive days exceeded 50%. After reaching the learning criterion, rats received either a selective DG lesion and/or a chronic recording implant.

Testing resumed 8 to 18 d after surgery on the same radial eight-arm maze in which the animals were pretrained. For animals without electrophysiological recording, at least 8 d of postsurgical testing were performed. For animals with electrophysiological recording, the animals were connected to a headstage and lightweight multiwire tether (see "Electrode turning" below) during testing after surgery, but the behavioral procedures were otherwise identical to presurgical training. Postsurgical testing was repeated daily until the animal performed at least four trials within 30 min per d regardless of the number of correct trials. Of 10 control animals, 6 animals required 1 d and 4 animals required 2 d to reach the criterion. Of 10 DG-lesioned animals, 8 and 2 animals required 1 d and 3 d to reach this criterion, respectively. After reaching this postsurgery criterion, training continued together with electrophysiological data collection. Behavioral procedures were identical to those without recordings except that the rats were required to perform 10–20 trials per d within a period of 60 min. Recordings were performed for at least 4 d.

Animal position and electrophysiological data were sampled using a digital Neuralynx recording system with a multichannel head-mounted preamplifier[2]. Differential recordings were performed with a dedicated reference electrode in the cortex. Unit recordings were filtered at 600 Hz to 6 kHz, and spike waveforms above an amplitude of 40 μV were time-stamped and recorded at 32 kHz for 1 ms. LFP recordings were filtered between 1 and 425 Hz. Sufficient common mode rejection to eliminate muscle artifacts in LFP recordings was confirmed by finding that ripple amplitude during immobility at reward was as weakly correlated as for sleep SWRs (Supplementary Fig. 6a,b). Despite the weak correlation of ripple amplitudes across recording channels, we also found coherence of high-frequency events across tetrodes (Supplementary Fig. 6c,d). The period during which the rat licked the chocolate milk reward was detected by a wire sensor that detected contact of the rat with the milk on each of the individual arms. The sensor detected the switch from an open-ended recording configuration to animal ground, and signals from these wires were digitized and timestamped by the Neuralynx recording system.

Distinct periods within a single trial of WM behavior were defined by the position and movement of the rat on the maze: (i) stem, <36 cm from the maze

center, (ii) outward, running outward in arm regions between 36 and 83 cm from the maze center, (iii) arm end 1, >83 cm from the maze center before reward consumption, (iv) reward, contact with reward sensors, (v) arm end 2, >83 cm from the maze center following the reward consumption period, and (vi) inward, running inward in arm regions between 36 and 83 cm from the maze center. For dentate recordings without reward sensors, periods iii–v were not analyzed separately. For illustration in figures, periods were normalized to the average of the period, and data from each trial were aligned according to their relative time within the period (Figs. 2f, 3g, 4d and 5b,d,g and Supplementary Fig. 5). For all analysis of neuronal activity patterns, only the initial visit to each of the eight arms was included and repeat visits were excluded (all excluded data are discussed in the associated Life Science Reporting Summary).

Surgical procedures. In all 37 animals, a single surgery was performed that included (i) bilateral intracranial infusions of colchicine or vehicle into the dorsal and ventral dentate gyrus, and/or (ii) chronic implantation of a tetrode array above the right hippocampus. At the time of surgery, the rat was anesthetized with isoflurane gas (2–2.5% in O_2 (20 mL /1 L per min)), and buprenorphine (0.05 mg/kg, s.c.) was given as an analgesic. For the DG lesion group, colchicine (2.5 mg/mL in phosphate buffer 0.1 M, pH 7.2) was injected into six sites (0.04 μL per site over 3 min) along the rostrocaudal axis of the dentate gyrus in each hemisphere at the following coordinates posterior of bregma, lateral of bregma, and ventral from dura (in mm): (i) −2.8, ±0.9 and −3.7; (ii) −4.0, ±2.1 and −3.6; (iii) −5.2, ±3.2 and −3.7; (iv) −5.2, ±3.2 and −7.6; (v) −6.2, ±4.2 and −3.7; (vi) −6.2, ±4.2 and −6.2. Infusions were made using a 1-μL Hamilton syringe, and the injection needle was left in place for at least 5 min to prevent spread. Colchicine has previously been shown to cause selective cell death of dentate granule cells[49–51]. For the sham group, the same amount of vehicle (phosphate buffer 0.1 M, pH 7.2) was injected into the same brain regions with the same procedure. In 21 animals, an electrode assembly consisting of 14 independently movable tetrodes was implanted above the right hippocampus (control group: 4.0 mm posterior and 2.7–2.9 mm lateral to bregma or 6.1 mm posterior and 4.2–4.6 mm lateral to bregma; DG lesion group: 3.5–4.4 mm posterior and 2.8–3.2 mm lateral to bregma). Tetrodes were constructed as previously described[52]. Before surgery, tetrode tips were plated with platinum to lower electrode impedances to 150–300 kΩ at 1 kHz. The recording device was secured to the skull using stainless steel screws and dental cement.

Electrode turning. Rats were connected to the recording equipment via AC-coupled unity-gain operational amplifiers close to the rat's head while resting on a towel in a large pot on a pedestal. One tetrode remained in the cortex as a reference, and another tetrode was lowered to the stratum lacunosum-moleculare to record hippocampal local field potentials. The remaining 12 tetrodes were advanced to the CA3 cell layer in the DG-lesioned animals or to the CA3 cell layer and the DG cell layer in control animals over a period of at least 2 weeks after surgery. The depth profile of the LFP was used as a guide for electrode movement. When the tetrodes approached the cell layer, further movement of the tetrodes was completed in small increments over several days. Once the tetrodes were adjacent to the cell layer, as indicated by the presence of low-amplitude multiunit activity, tetrodes were not turned again and were allowed to settle into the cell layer for stable recordings over a period of many days. Tetrode recording locations were confirmed postmortem. DG lesions resulted in substantial tissue loss within DG, which shifted the coordinates for CA3 recording sites and reduced the yield compared to controls.

Random foraging (RF) task. Seven control animals and nine DG-lesioned animals performed a random foraging (RF) task on the radial arm maze. After completion of the WM task, the rat was allowed to rest for 5–20 min, during which the floor of the maze was cleaned with water. The rat was then allowed to freely forage for randomly scattered cocoa puffs for 10 min on the entire maze. The RF task was performed at least once per day and repeated for at least 2 consecutive days.

Linear track task. After completing electrophysiological recordings in the WM and RF tasks, 3 control animals and 3 DG-lesioned animals were tested on a linear track in a different room. One DG-lesioned animal was subject to only the linear track task. Animals were trained to run back and forth on a linear track (148 × 7 cm with shallow side walls rising 0.5 cm above the surface of the arm, elevated 53 cm above the floor) to obtain chocolate milk reward at the ends of the track for three or four 10-min sessions with an intertrial interval of 5 min. Sensors at each reward site indicated when the reward was consumed, as described for the WM task.

Behavioral periods were divided and defined as follows: (i) toward reward, movement toward reward between the center and >20 cm from an arm end, (ii) track end 1, <20 cm from an arm end before reward, (iii) reward, contact with reward sensor, (iv) track end 2, <20 cm from the end after reward, and (v) from reward, >20 cm from the arm end to center of arm. For illustration in figures, each period was normalized to the average for the period, and data from each trial were aligned according to their relative time within the normalized period (Supplementary Fig. 13f,g).

Sharp-wave ripple detection. Sharp waves co-occur with ripples near the cell layer[11,22]. For the detection of ripples, LFP signals were bandpass-filtered at 150–250 Hz and the root-mean-square power was calculated in the ripple-band with a bin size of 10 ms. The threshold for awake-ripple detection was set to 3–5 s.d. above the mean[17]. Onset and offset of ripples was marked at the points when the ripple power first exceeded and dropped below 3 s.d. above the mean, and events with a duration of <15 ms were excluded. To calculate incidence rates for each behavioral period (for example, reward), the total number of ripples was divided by the average duration of the corresponding period over all trials. In addition, the ripple rate during reward consumption in the WM task was also compared to the ripple rates during the immobility period at arm ends before and after reward consumption (defined as running speed < mean running speed during reward; Fig. 4e and Supplementary Fig. 9d). The ripple rate during reward consumption was normalized by ripple rates at track ends before reaching the reward on the linear track (Supplementary Fig. 13i).

LFP spectrum analysis. To compute the time–frequency representation of LFP power, LFP signals were convolved by a Morlet wavelet family defined by a constant ratio of $F_0/\sigma_F = 7$, where F_0 represents the frequency of interest and σ_F is the bandwidth of the wavelet in the frequency domain. The absolute power spectrum of the LFP during each 1-ms time window was calculated, and z-scores were computed for each frequency band using the mean and s.d. of the power measured across the entire behavioral session for each tetrode. For constructing the representative behavior-related LFP power spectra in Figs. 3e and 5b and Supplementary Fig. 7a,b, the original time–frequency LFP power spectra were stretched or compressed in time, such that they matched the average time the animal spent in the different behavioral periods (for example, reward) over the entire session. The normalized data were then averaged across all trials. Oscillations in the gamma band were divided into the 20- to 50-Hz range and mid/fast gamma range (65–140 Hz). A 20-Hz cutoff was used to avoid confounds with theta harmonics (14–18 Hz) but to include frequency bands that have been referred to as 20–40 Hz or beta[43–45]. Because we found that the firing rates of CA3 cells were low during 20- to 50-Hz oscillations in the reward zone, we considered these oscillations mechanistically different from CA3-generated slow gamma oscillations, and refer to these oscillations by their frequency band. For quantification of each frequency band, the z-scored power was averaged separately for each behavioral period. To estimate the relationship between running speed and oscillations, z-scored power of each frequency and the velocity of animals were calculated during each 300-ms time window.

Coherence between two electrodes was computed using a multitaper method from the Chronux Matlab toolbox (http://chronux.org/) with a window size of 0.5 s and 5 tapers. For quantification, across behavioral periods data were averaged across all DG–CA3 pairs.

Spike sorting. Spike sorting was performed offline using a modified version of the graphical cluster-cutting software MClust[53]. Sleep recordings before and after the behavioral experiments were included in the analysis to assure recording stability throughout the experiment and to identify hippocampal cells that were silent during behavior. Autocorrelation and cross-correlation functions were used as additional separation criteria. CA3 cells with an average firing rate of less than 3 Hz and waveforms longer than 200 μs were considered to be putative excitatory cells and included in analysis. DG cells with an average firing rate of less than 3 Hz and waveforms longer than 150 μs were considered to be putative DG granule or mossy cells.

DG cell firing properties. For each DG cell, average firing rates were calculated in (i) inner areas <83 cm from the maze center and (ii) arm end areas >83 cm from the maze center (Fig. 2b–e). The activity patterns of a cell were considered selective for inner areas, both areas or arm end areas if the ratio of the average firing rate in inner area to the average firing rate in end area was >150%, 66.6–150% or <66.6%, respectively. A cell was defined as silent if the firing rate during the WM task was <0.01 Hz. To quantify the spatial selectivity of DG cell firing, we created two $N \times 8$ arms matrices of firing rates, one for the inner segments and one for the arm ends. With each of the matrices, we conducted repeated-measures ANOVA with factors arms and trials to measure arm selectivity. The ANOVA were performed for each DG cell separately, and cells with $P < 0.05$ were considered spatial.

CA3 place cell firing properties. Spatial firing-rate distributions for each well-isolated neuron were constructed by dividing the total number of spikes in each location bin (10×10 cm) by the amount of time that the animal spent in that location. Data were then smoothed by a two-dimensional convolution with a Gaussian kernel with a s.d. of one pixel (10 cm), and the peak firing rate was the maximum firing rate in any of the pixels. In addition, the average firing rate was calculated across all trials in the WM task, and cells with an average firing rate of <0.05 Hz in behavior were excluded from further analysis. To describe place field properties, we calculated information per spike and sparsity of hippocampal place cells as previously described[54].

For spatial correlation analysis, firing patterns of individual cells were compared between trials[2,55]. For each cell, a separate spatial map was calculated

for each trial, and the Pearson correlation coefficient between firing rates in corresponding pixels was calculated between all trial pairs. All pairwise correlation coefficients were then averaged. Spatial maps between the WM and the RF tasks were compared by first generating a spatial map averaged across all trials in the WM task and a spatial map for the entire 10-min recording session in the RF task, and by then calculating Pearson's correlation coefficient between the two maps.

Prospective ratio. Prospective firing was tested in CA3 cells that had place fields on select arms of the WM task. To determine arm-specific firing of each CA3 cell, average firing rates in individual arms (including the reward location) were calculated across all trials. For each cell, we then defined preferred arms as those in which the cell's firing rate in one arm was >0.5 Hz and at least 2.0 times higher than the firing rate averaged over all the other arms. If two preferred arms per cell were found, the arms with the higher and lower firing rates were defined as the primary and secondary preferred arm, respectively. Spikes that occurred during reward consumption before visiting the primary arm were defined as prospective spikes, and spikes that occurred during reward consumption after visiting the primary arm were defined as retrospective spikes. To not confound reward-related with spatial firing, both the primary and secondary arms were excluded from reward related calculations. Due to the limited sampling duration at reward locations within a single trial, we pooled prospective spikes and pooled retrospective spikes over all trials (10–20 trials) of a recording session and normalized them by the total amount of time the rat spent in reward periods. Note that the interaction between the sequence of arm visits and the location of the field did not bias our results, as recordings included 10–20 trials in which the sequence of arm visits was randomized between trials. The likelihood that the visit to the arm with the place field occurred early or late in the trial was therefore counterbalanced. For each cell, we then calculated a prospective ratio (difference between prospective and retrospective firing rate divided by the sum of both rates)[15]. The ratio ranged between –1 and +1, with a positive value indicating a cell's bias toward representing future positions while the rat is at reward locations. In addition, the relative timing of firing compared to ripple generation was examined with cross-correlograms (10 ms bin size) between CA3 firing and reward-associated ripple events (Fig. 7c).

Postmortem histology. Electrodes were not moved after the final recording session. Rats received an overdose of sodium pentobarbital and were perfused intracardially with ~200 mL of 0.37% sulfide solution (49 mM Na_2S and 86 mM NaH_2PO_4, pH 7.2) or phosphate buffered saline (PBS) for 10 min, and 200 mL of 4% paraformaldehyde in PBS (pH 7.4) for 10 min. To aid the reconstruction of electrode tracks, the electrodes were not withdrawn from the brain until 3–4 h after perfusion. Brains were then extracted, placed in 4% paraformaldehyde overnight, and transferred to 30% sucrose in phosphate buffered saline until equilibrated. Frozen coronal sections (40 μm) were cut using a microtome, and serial sections were mounted. Sections for 10 recording animals were stained with cresyl violet, sections from 11 dentate-lesioned recording animals were stained with Timm's sulfide silver and cresyl violet, and sections from the 16 animals with only behavioral testing were immunostained with NeuN. Cresyl violet stain was used to label all hippocampal cells with a counterstain in order to facilitate the verification of recording tetrode locations and the quantification of the dentate lesions (Figs. 2a and 3a). NeuN immunostain was used to label all hippocampal neurons to quantify the dentate lesions in behavioral animals (Fig. 1c). Timm stain was used to label mossy fiber (MF) projections from the dentate granule neurons to the CA3 pyramidal neurons in black[56,57], which was used in DG-lesioned rats to score any degree of remaining mossy fiber innervation within the CA3 stratum lucidum (Fig. 4b).

For combined cresyl violet and Timm staining, slide-mounted sections were first placed in a developer solution for ~75 min in darkness at room temperature (20–25 °C)[56,57]. The developer solution consisted of 120 mL gum arabic solution (500 g gum arabic/L water), 60 mL hydroquinone solution (3.41 g hydroquinone), 10 mL citrate buffer (2.55 g citric acid, 2.06 g sodium citrate), and 1 mL silver nitrate solution (0.17 g silver nitrate). The slices were then rinsed in water and counterstained with cresyl violet. For NeuN immunostaining, immunoperoxidase procedures were performed on every sixth free-floating section. After 1 h of incubation in blocking solution (5% horse serum and 0.25% Triton X-100 in PBS) antibody incubations were done in PBS at room temperature overnight. The following antibodies were used: NeuN (mouse monoclonal; 1:15,000; Millipore: MAB377) and biotinylated anti-mouse (1:1,000; Vector Laboratories: BA-2000). The immune reaction was amplified by 1-h incubation with an ABC kit (1:1,000; Vector Laboratories: PK-6100) and developed with 3,3′-diaminobenzidine substrate (DAB; 0.5 mg/mL; AMRESCO: E733) for 100 s. At the end of the staining procedures, all tissue was coverslipped using Permount (Fisher Scientific: SP15-500).

Three-dimensional reconstruction of the tetrode array. For histology from animals in electrophysiological recording experiments, each section through segments of the hippocampus with electrode tracks was collected. All tetrodes of the 14-tetrode bundle were identified by matching tetrode positions in the bundle with electrode tracks in postmortem tissue[2,55]. Recordings from a tetrode

were included in the data analysis if the tetrode's deepest position could be clearly assigned to either DG or CA3 (Figs. 2a, 3a and 4a and Supplementary Fig. 2).

Quantification of DG lesion and mossy fiber score. The volume of the granule cell layer was measured in NeuN-labeled and cresyl violet-positive sections throughout the entire dorsoventral extent of the DG with computer-based 3D volumetry. Lesion accuracy and quality were quantified using the Cavalieri estimator application in Stereo Investigator software (grid spacing of 20 μm, 10× objective) for volume quantification of the granule cell layer. The remaining granule cell volume of each DG-lesioned animal was normalized to a control volume of $430 \times 10^7\,\mu m^3$ ($n = 5$ animals). For measurements of lesions with cresyl violet-stained tissue, the estimate of the remaining DG granule cell volume can be expected to be an upper bound for the proportion of remaining granule cells, because stained nongranule cells, such as glia, were also counted as remaining volume. CA3 and CA1 hippocampal subregions were also inspected in the DG-lesioned animals (Supplementary Fig. 1c).

For recording animals with DG lesions, any remaining granule cell innervation was quantified by examining the Timm staining of MFs at CA3 recording sites. The distribution of Timm-positive signal at each tetrode tip in the CA3 striatum lucidum was scored according to the following criteria (Fig. 4b):

0. No Timm-positive staining (black reaction products). Signals comparable to background intensity in neighboring areas such as the CA3 stratum radiatum and stratum lacunosum-moleculare.
1. Weak Timm-positive labeling. Less than 50% of Timm-positive layer thickness and less than 30% of Timm-positive signal intensity, compared to control sections.
2. Moderate Timm-positive labeling. More than 50% of Timm-positive layer thickness, but less than 70% of Timm-positive signal intensity, compared to control sections.
3. Abundant Timm-positive labeling. More than 50% of Timm-positive layer thickness and more than 70% of Timm-positive signal intensity, compared to control slices.
4. Control (no DG lesion).

The scores above were combined into two groups: scores of 0 and 1 were classified as the low-density MF group (LMF), and scores of 2 were classified as the high-density MF group (hMF). No tetrodes in lesioned rats received a score of 3.

For analysis by CA3 subregions, we defined CA3c as the area of the CA3 pyramidal cell layer between the two blades of the dentate granule cell layer. The remaining area of the CA3 pyramidal cell layer was defined as CA3a,b. In control animals, 8 and 9 tetrodes were located at CA3a,b and CA3c, respectively. In DG-lesioned animals, 12 and 12 tetrodes were located at CA3a,b and CA3c, respectively.

Statistical analysis. Unless specified otherwise, both correct and incorrect trials were included in all reported analyses. If incorrect trials were included, only the first entry into the arm (i.e., when reward was present) was included in the

analysis. All data are presented as mean ± s.e.m. and were analyzed using Matlab. Two-sample comparisons were performed by two-sided t test or, if the data did not meet the assumptions of the t test, were analyzed with the nonparametric two-sided Mann–Whitney U-test. Multiple group comparisons of normalized ripple rates were assessed using a repeated-measures ANOVA, followed by Scheffé test when necessary. Multiple group comparisons of mean firing properties were performed by Mann–Whitney U-test followed by post hoc Bonferroni corrections. The null hypothesis was rejected at $P < 0.05$. No statistical methods were used to predetermine sample sizes, but our sample sizes are similar to those reported in previous publications[58]. Data collection and analysis were not performed blind to the conditions of the experiments.

Life Sciences Reporting Summary. Further information on experimental design is available in the Life Sciences Reporting Summary.

Data and code availability. The data and code that support the findings of this study are available from the corresponding author upon reasonable request.

References

49. Walsh, T. J., Schulz, D. W., Tilson, H. A. & Schmechel, D. E. Colchicine-induced granule cell loss in rat hippocampus: selective behavioral and histological alterations. *Brain Res.* **398**, 23–36 (1986).
50. Goldschmidt, R. B. & Steward, O. Preferential neurotoxicity of colchicine for granule cells of the dentate gyrus of the adult rat. *Proc. Natl Acad. Sci. USA* **77**, 3047–3051 (1980).
51. Goldschmidt, R. B. & Steward, O. Neurotoxic effects of colchicine: differential susceptibility of CNS neuronal populations. *Neuroscience* **7**, 695–714 (1982).
52. Brandon, M. P., Koenig, J., Leutgeb, J. K. & Leutgeb, S. New and distinct hippocampal place codes are generated in a new environment during septal inactivation. *Neuron* **82**, 789–796 (2014).
53. Redish, A.D. MClust 3.5, freeware spike sorting. http://redishlab.neuroscience.umn.edu/MClust/MClust.html (2009).
54. Skaggs, W. E., McNaughton, B. L., Wilson, M. A. & Barnes, C. A. Theta phase precession in hippocampal neuronal populations and the compression of temporal sequences. *Hippocampus* **6**, 149–172 (1996).
55. Koenig, J., Linder, A. N., Leutgeb, J. K. & Leutgeb, S. The spatial periodicity of grid cells is not sustained during reduced theta oscillations. *Science* **332**, 592–595 (2011).
56. Cavazos, J. E., Golarai, G. & Sutula, T. P. Mossy fiber synaptic reorganization induced by kindling: time course of development, progression, and permanence. *J. Neurosci.* **11**, 2795–2803 (1991).
57. Buckmaster, P. S. & Dudek, F. E. Network properties of the dentate gyrus in epileptic rats with hilar neuron loss and granule cell axon reorganization. *J. Neurophysiol.* **77**, 2685–2696 (1997).
58. Schlesiger, M. I. et al. The medial entorhinal cortex is necessary for temporal organization of hippocampal neuronal activity. *Nat. Neurosci.* **18**, 1123–1132 (2015).

Corresponding Author: Jill K. Leutgeb

Date: November 30, 2017

Life Sciences Reporting Summary

Nature Research wishes to improve the reproducibility of the work we publish. This form is published with all life science papers and is intended to promote consistency and transparency in reporting. All life sciences submissions use this form; while some list items might not apply to an individual manuscript, all fields must be completed for clarity.

For further information on the points included in this form, see Reporting Life Sciences Research. For further information on Nature Research policies, including our data availability policy, see Authors & Referees and the Editorial Policy Checklist.

▶ Experimental design

1. Sample size

   Describe how sample size was determined.

   > Sample size (the number of rats) was determined by previous publications that performed the behavioral task used in our study (McLamb et al., Neurotoxicology, 1988) and by the expected number of active neurons that can be recorded from the dentate gyrus (DG) and CA3 pyramidal layer from awake-behaving, Long-Evans rats (Leutgeb et al., Science, 2007). Numbers of neurons needed for statistical analysis were based on previous publications using the same measures (Oliva et al., Neuron, 2016; Carr et al., Neuron, 2012; Leutgeb et al., Science, 2005). Main effects were highly significant with the number of recording sites and cells in each group, and the effects were consistent across individual rats and cells within each group. Individual data is presented frequently throughout the paper to document the consistency of the effects. In CA3 recording animals, fewer control rats were needed in comparison to DG-lesioned rats as more tetrodes could be accurately placed in the CA3 cell layer which yielded more data per animal. DG lesions resulted in substantial tissue loss within the DG which shifted the coordinates for CA3 recording sites differently for each DG lesioned animal. Although the coordinates were adjusted in lesioned animals, it was more challenging to consistently place tetrodes in the CA3 layers in these animals compared to controls. Therefore, the DG lesion group was larger in order to compensate for the variation in lesion size and subsequent tissue shrinkage.

2. Data exclusions

   Describe any data exclusions.

   > For all trials and all animals, we only analyzed data from the first visit to each of the eight arms. Reentries into a previously visited arm were counted as errors but were not included in the analysis for the following reasons: (1) It would result in an imbalance in the number of analyzed arms. (2) Reward was only present during the first visit, and including subsequent visits in the analysis would thus generate an imbalance by adding instances without reward consumption. The restriction of the analysis to the initial arm visit is explicitly mentioned in the Methods and Results sections.
   >
   > Excluded from analysis were behavioral trials that were not completed by an animal. A trial ended when the rat had retrieved the reward from all 8 arms and returned to the stem, or if the total time in one trial exceeded 10 min. When a trial was stopped for exceeding the time limit, it was removed from analysis.
   >
   > All thresholds and criteria used for data analysis are clearly described in the Online Methods.

3. Replication

   Describe whether the experimental findings were reliably reproduced.

   > All attempts at replication were successful. Main effects were consistent across individual rats and cells within each group.

4. Randomization

   Describe how samples/organisms/participants were allocated into

   > Rats were purchased from Charles River Laboratory. Littermates were

experimental groups.

divided and randomly assigned to control groups, dentate-lesioned groups, and recording groups. Groups were run in parallel in groups of 4-6 or 2-3 for behavioral and recording experiments respectively.

5. Blinding

Describe whether the investigators were blinded to group allocation during data collection and/or analysis.

Investigators quantifying TIMM staining followed the criteria outlined in the Online Methods and were blind to group. Otherwise, data collection and analysis were not performed blind to the conditions of the experiments.

Note: all studies involving animals and/or human research participants must disclose whether blinding and randomization were used.

6. Statistical parameters

For all figures and tables that use statistical methods, confirm that the following items are present in relevant figure legends (or the Methods section if additional space is needed).

n/a	Confirmed	
☐	☒	The <u>exact</u> sample size (n) for each experimental group/condition, given as a discrete number and unit of measurement (animals, litters, cultures, etc.)
☐	☒	A description of how samples were collected, noting whether measurements were taken from distinct samples or whether the same sample was measured repeatedly.
☐	☒	A statement indicating how many times each experiment was replicated
☐	☒	The statistical test(s) used and whether they are one- or two-sided (note: only common tests should be described solely by name; more complex techniques should be described in the Methods section)
☐	☒	A description of any assumptions or corrections, such as an adjustment for multiple comparisons
☐	☒	The test results (e.g. p values) given as exact values whenever possible and with confidence intervals noted
☐	☒	A summary of the descriptive statistics, including central tendency (e.g. median, mean) and variation (e.g. standard deviation, interquartile range)
☐	☒	Clearly defined error bars

See the web collection on statistics for biologists for further resources and guidance.

▸ Software

Policy information about availability of computer code

7. Software

Describe the software used to analyze the data in this study.

We have stated where computer generated code can be found that was used in the manuscript. For example: Chronux Matlab toolbox (Online Methods). MClust cluster cutting software (Available at http://redishlab.neuroscience.umn.edu/MClust/MClust.html; Online Methods).
All offline computational analyses were performed using MATLAB 7.9.0 2009B. Each analysis procedure is described in necessary detail within the "Data Analysis" section of the Online Methods for others to execute. In the description of analysis methods, more detail is provided for novel analysis methods. Any analysis MATLAB code will be deposited on a server and is available by sending a request to the corresponding author. A data availability and code availability statement can be found in the Online Methods.

For all studies, we encourage code deposition in a community repository (e.g. GitHub). Authors must make computer code available to editors and reviewers upon request. The *Nature Methods* guidance for providing algorithms and software for publication may be useful for any submission.

▸ Materials and reagents

Policy information about availability of materials

8. Materials availability

Indicate whether there are restrictions on availability of unique materials or if these materials are only available for distribution by a for-profit company.

No unique materials were used. All materials were available from commercial sources which are listed in the Online Methods. Any custom analysis MATLAB code not already freely available online (see question #7) is available from the corresponding author upon request.

9. Antibodies

Describe the antibodies used and how they were validated for use in the system under study (i.e. assay and species).

Antibody specifics including company and catalog name are reported in the Online methods. The following antibodies were used: NeuN (mouse monoclonal; 1:15000; supplier = Millipore: catalog # = MAB377, clone = A60, lots = LV1616015 and 2326372) and biotinylated anti-mouse (1:1000; supplier = Vector Laboratories: catalog # = BA-2000, clone = horse polyclonal, lots = V0522, X0920, and X1103). Antibodies have been validated for use in the system under study in previously published data. R.J. Mullen, C.R. Buck, A.M. Smith NeuN, a neurona, specific nuclear protein in vertebrates Development, 116 (1992).

10. Eukaryotic cell lines
   a. State the source of each eukaryotic cell line used.

   No Eukaryotic cell lines were used in the study.

   b. Describe the method of cell line authentication used.

   No Eukaryotic cell lines were used in the study.

   c. Report whether the cell lines were tested for mycoplasma contamination.

   No Eukaryotic cell lines were used in the study.

   d. If any of the cell lines used in the paper are listed in the database of commonly misidentified cell lines maintained by ICLAC, provide a scientific rationale for their use.

   No Eukaryotic cell lines were used in the study.

▶ Animals and human research participants

Policy information about studies involving animals; when reporting animal research, follow the ARRIVE guidelines

11. Description of research animals

Provide details on animals and/or animal-derived materials used in the study.

A total of 37 male Long Evans rats (3-6 months old) were used in this study. The animals were housed individually and maintained on a 12-h light/12-h dark schedule with lights off at 6:00 AM. All animals were obtained from Charles River Laboratory. All surgical and experimental procedures were approved by the Institutional Animal Care and Use Committee at the University of California, San Diego, and conducted according to National Institutes of Health guidelines.

Policy information about studies involving human research participants

12. Description of human research participants

Describe the covariate-relevant population characteristics of the human research participants.

No human research participants were involved in the study.